# NHR-23 activity is necessary for developmental progression and apical extracellular matrix structure and function

Londen C. Johnson[1], An A. Vo[1], Jack C. Clancy[1], Joseph Aguilera[1], Max T. Levenson[1], Chloe Wohlenberg[1], Andreas Rechtsteiner[1], James Matthew Ragle[1], and Jordan D. Ward[1‡].

[1]Department of Molecular, Cell, and Developmental Biology, University of California-Santa Cruz, Santa Cruz, CA 95064, USA.

[‡]Author for correspondence.

Corresponding author email: jward2@ucsc.edu

Keywords: *C. elegans*, molting, NHR-23, nuclear hormone receptor, apical extracellular matrix, auxin-inducible degron

Running Title: NHR-23 in *C. elegans* molting

**Summary Statement**

This work provides insight into when and where the transcription factor NHR-23 acts to promote apical extracellular matrix structure, function and remodeling in *C. elegans.*

## ABSTRACT

Nematode molting is a remarkable process where animals must repeatedly build a new apical extracellular matrix (aECM) beneath a previously-built aECM that is subsequently shed. The nuclear hormone receptor NHR-23/NR1F1 is an important regulator of *C. elegans* molting. NHR-23 expression oscillated in the epithelium, closely following the reported mRNA expression. Soma-specific NHR-23-depletion caused severe developmental delay and tissue-specific RNAi suggested that *nhr-23* acts primarily in seam cells. NHR-23 coordinates the expression of factors involved in molting, lipid transport/metabolism, and remodeling of the aECM. NHR-23 depletion caused dampened expression of a *nas-37* promoter reporter and a loss of reporter oscillation. The collagen ROL-6 and zona pellucida protein NOAH-1 displayed aberrant annular localization and severe disorganization over the seam cells following NHR-23 depletion. The expression of the adult cuticle-specific collagen BLI-1 was diminished and frequently found in patches. Consistent with these localization defects, the cuticle barrier was severely compromised. Together, this work provides insight into how NHR-23 acts in the seam cells to coordinate aECM regeneration during development.

## INTRODUCTION

Molting is a critical developmental process required for the growth of all ecdysozoans, a clade comprising an estimated total of 4.5 million living species (Telford et al., 2008). Although specific to invertebrates, molting involves conserved processes such as apical extracellular matrix (aECM) remodeling, intracellular trafficking, and oscillatory gene expression (Lažetić and Fay, 2017). Molting is also a process of interest for developing new drugs against parasitic nematodes (Ghedin et al., 2007). Parasitic nematodes cause over a billion human infections each year and loss of livestock and crops (Ward, 2015b). However, very few drugs exist and resistance to those drugs is emerging rapidly (Ward, 2015b). While many genes involved in nematode molting have been identified in *C. elegans* (Frand et al., 2005), little is known about how their gene products are coordinated to promote aECM remodeling and the generation and release of a new cuticle.

Nematodes progress through four periodic larval stages (L1-L4), prior to becoming a reproductive adult (Brenner, 1974). The end of each larval stage is punctuated by a molt that involves trafficking and secretion of aECM components, assembly of a new aECM underneath the old cuticle, followed by separation of the cuticle from the underlying aECM (apolysis) and shedding of the old cuticle (ecdysis)(Lažetić and Fay, 2017). Apolysis coincides with a sleep-like behavior called lethargus (Singh and Sulston, 1978). The cuticle is a collagenous exoskeleton secreted by hypodermal and seam epithelial cells (Page and Johnstone, 2007). The outermost layer (glycocalyx) is rich in carbohydrates and mucins and thought to be secreted by the excretory gland cell (Nelson et al., 1983; Singh and Sulston, 1978). Beneath the glycocalyx is the glycolipid- and lipid-rich epicuticle which is postulated to function as a hydrophobic surface barrier (Blaxter, 1993; Blaxter et al., 1992). Underlying the epicuticle is a layer comprised mainly of cuticlin proteins. Between the epidermal membrane and the epicuticle are collagen rich layers, including a fluid-filled medial layer with collagen struts (Lažetić and Fay, 2017; Page and Johnstone, 2007). Sets of collagens oscillate in expression over the course of each molt and are classified into three groups based on temporal expression: early, intermediate, and late collagens (Johnstone and Barry, 1996; Page and Johnstone, 2007). While the specific localization of most collagens is unknown, collagens from the same group are thought to be in the same layer. A transient structure, the sheath or pre-cuticle, is formed during each larval stage and thought to pattern the cuticle (Cohen and Sundaram, 2020). Many of the components of this pre-cuticle are related to mammalian matrix proteins. The *C. elegans* pre-cuticle contains Zona Pellucida proteins, proteins related to small leucine-rich proteoglycans, and lipid transporters in the lipocalin family (Cohen and Sundaram, 2020; Cohen et al., 2020; Forman-Rubinsky et al., 2017; Kelley et al., 2015; Sapio et al., 2005; Vuong-Brender et al., 2017).

Nuclear hormone receptor (NHR) transcription factors are key regulators of molting in insects and nematodes (King-Jones and Thummel, 2005; Taubert et al., 2011). NHRs are characterized by a ligand-binding domain (LBD) which has the potential to bind small molecules such as ligands and dietary-derived metabolites (Taubert et al., 2011). Not all

NHRs have known ligands, though the ancestral proteins from which all NHRs descend can bind ligands (Bridgham et al., 2010; Eick and Thornton, 2011). NHRs have a canonical zinc finger DNA-binding domain (DBD) with an unstructured hinge region between the DBD and LBD that is subject to post-translational regulation (Antebi, 2015; Campbell et al., 2008; Ward et al., 2013). A single, conserved nuclear hormone receptor, NHR-23/NR1F1 (hereafter referred to as NHR-23), an ortholog of DHR3 in insects and ROR$\alpha$ in mammals, is a key regulator of *C. elegans* molting. *nhr-23* mutation or inactivation by RNAi leads to embryonic lethality, larval arrest, ecdysis defects, and morphology defects (Frand et al., 2005; Gissendanner et al., 2004; Kostrouchova et al., 1998; Kostrouchova et al., 2001). *nhr-23* mRNA expression oscillates over the course of each larval stage, peaking mid-larval stage and hitting a trough at the molt (Gissendanner et al., 2004; Kostrouchova et al., 2001). Experiments with *nhr-23* mutants and RNAi have demonstrated a role for NHR-23 in all four larval molts (Kostrouchova et al., 1998; Kostrouchova et al., 2001). The NHR-23 insect ortholog (DHR3) is part of the molting gene regulatory network (Lam et al., 1997; Ruaud et al., 2010) and the mammalian ortholog (RORα) regulates circadian rhythms, lipid metabolism, and immunity (Jetten, 2009).

We found that NHR-23 protein oscillates and rapid NHR-23 depletion via an auxin-inducible degron causes severe developmental delay. Analysis of NHR-23 target genes suggests a role in coordinating aECM assembly, remodeling, and construction of specific cuticular structures. NHR-23 depletion causes aberrant localization of the collagens ROL-6 and BLI-1 and of the pre-cuticle factor NOAH-1. NHR-23 activity is necessary in seam cells to promote molting and timely development. Our work provides an entry point into understanding how NHR-23 coordinates the complex cell biology underpinning molting.

## RESULTS

### NHR-23 oscillates during development

Expression of *nhr-23* mRNA oscillates throughout each larval stage of the *C. elegans* life cycle (Gissendanner et al., 2004; Hendriks et al., 2014; Kostrouchova et al., 2001; Meeuse et al., 2020) reaching peak expression mid-intermolt and a trough prior to the

completion of the next molt (Fig. 1A). However, mRNA expression profiles do not always match protein levels (de Sousa Abreu et al., 2009; Vogel and Marcotte, 2012). To determine whether NHR-23 protein oscillates, we monitored the expression of the endogenous NHR-23::GFP, over 28 hours. During L1, oscillating expression of NHR-23::GFP was observed in the nuclei of seam and hypodermal cells (Fig. S1). Expression of NHR-23 rises and falls prior to the completion of the 1$^{st}$ molt; this pattern is repeated prior to the 2$^{nd}$ molt as well (Fig. 1B,C), similar to the reported mRNA expression (Gissendanner et al., 2004; Kostrouchova et al., 2001). As GFP tags can affect the expression or stability of proteins (Agbulut et al., 2006; Baens et al., 2006), we assayed the expression of NHR-23 through western blotting time-courses using an *nhr-23::AID*::3xFLAG* strain (Zhang et al., 2015). These experiments confirmed that NHR-23::AID*::3xFLAG also oscillates (Fig. 1C), similar to our NHR-23::GFP imaging experiments (Fig. 1B). We detected three distinct NHR-23 bands; the lowest band is consistent with the size of NHR-23b/f (Fig. 1C,D, Fig. S2). The upper two bands are larger than expected, which could reflect post-translational modification or that NHR-23 migrates aberrantly during SDS-PAGE. All observed NHR-23 bands oscillate, though the lowest band was expressed more strongly than the other bands (Fig. 1C).

**Distinct phenotypes caused by early or late NHR-23-depletion in L1 larvae**

Given that NHR-23 oscillates, we tested when NHR-23 was necessary for molting during the L1 larval stage. We have previously shown that the auxin-inducible degron system can rapidly deplete a nuclear hormone receptor (NHR-25), with almost complete depletion within 30 minutes (Zhang et al., 2015). In a pilot experiment, we consistently found weaker depletion phenotypes using an *nhr-23::GFP::AID*::3xFLAG* strain (Ragle et al., 2020) compared to the *nhr-23::AID*::3xFLAG strain* (Zhang et al., 2015)(Table S1). We therefore transitioned to using the *nhr-23::AID*::3xFLAG* strain for all experiments involving phenotypic analysis. We first tested NHR-23::AID*::3xFLAG depletion kinetics and found robust depletion within 15 minutes after exposure to 4 mM auxin and levels remained low over the 16 hour time course (Fig. 2B).

We performed timed depletion experiments in the L1 larval stage (Fig. 2A) using an *eft-3p::TIR1::mRuby2* control strain (henceforth referred to as *TIR1*) and a strain that permits somatic depletion of NHR-23 in the presence of auxin, (*eft-3p::TIR1::mRuby2; nhr-23::AID*::3xFLAG;* henceforth referred to as *nhr-23::AID*; *TIR1*). Synchronized L1s were shifted onto either 4 mM auxin or control plates every two hours (Figure 2A). Animals were scored for molting defects at 20 hours post-release. 100% of *TIR1* control animals shifted onto control or auxin plates successfully molted and transitioned into the second larval stage. *nhr-23::AID*; *TIR1* animals shifted onto control plates also reached the L2 stage, indicating that ethanol does not affect developmental timing in this context. In contrast, *nhr-23::AID*; *TIR1* animals shifted onto auxin displayed multiple phenotypes including molting defects, internal vacuoles, developmental abnormalities such as disrupted tails and viable animals with a squashed morphology ("splatter")(Fig. 2C). We then quantified the molting defects, scoring animals unable to shed their cuticles, or with morphological abnormalities (Fig. 2D). Vacuoles were observed in both the *TIR1* control and *nhr-23::AID; TIR1* strains. This could be a result of exposure to auxin or possibly an effect of the imaging process. We did not pursue the vacuole phenotype further. The percentage of *nhr-23::AID*; *TIR1* animals with unshed cuticles was low (5%) when animals were shifted to auxin 2 hours post-release (Fig. 2D). This percentage increased the later animals were shifted to auxin, reaching a maximum of 58% when animals were shifted 12 hours post-release (Fig. 2D). The majority of *NHR-23::AID; TIR1* animals shifted on to auxin at the 14 and 16 hour time points appeared wild type (Fig. 2D). *TIR1* and *nhr-23::AID; TIR1* animals grown on control plates developed normally with no arrest or morphological defects (n=35 for each strain). We repeated the 16 hour shift experiment and scored animals 48 hours later. Based on size, gonadal morphology, and vulval morphology, animals were L2 and L3 larvae (Figure S4). These data suggest that NHR-23 is necessary during the 4-12 hour post-release window to promote the L1 molt, then is dispensable during the 14-16 hour post-release window.

**NHR-23 depletion causes severe developmental delay**

*nhr-23::AID*; *TIR1* animals exposed to auxin at hours 2 and 4 appeared smaller than control animals and had fewer molting defects than animals shifted onto auxin between

6-12 hours. To test whether early depletion caused a developmental arrest, we used an *hlh-8p::GFP* promoter reporter to monitor the M lineage (Harfe et al., 1998). Newly hatched L1 animals have one M cell which undergoes a stereotypical series of divisions to produce 16 M lineage cells by the L1 molt (Fig. S5)(Sulston and Horvitz, 1977). We shifted synchronized *nhr-23::AID*; *TIR1* animals carrying an *hlh-8p::GFP* reporter onto auxin plates at 3 hours and 9 hours post-release. We imaged animals 24 hours post-release and M cell number was scored (Fig S4B,C). *nhr-23::AID*; *TIR1* animals exposed to auxin 3 hours post-release had an average count of 13.45 M cells while the late exposure resulted in an average of 15.55 M cells (Fig. S4B). The *nhr-23::AID*; *TIR1* animals exposed to auxin 9 hours post release did not have significantly different M cell number than any of the controls ($p>0.3$)(Fig. S4C). These data suggest that *nhr-23::AID*; *TIR1* animals exposed to auxin 3 hours post release were late L1 larvae. There are well-characterized developmental checkpoints that promote larval arrest in the absence of food (Fielenbach and Antebi, 2008; Kaplan and Baugh, 2016). *daf-16* is a transcription factor which is part of the insulin signaling pathway and is necessary for starvation-induced L1, L3, and L4 arrest (Baugh and Sternberg, 2006; Schindler et al., 2014). Starved *daf-16* mutants fail to arrest at these checkpoints and continue development (Baugh and Sternberg, 2006; Schindler et al., 2014). d*af-16* mutation did not significantly alter M cell number when NHR-23 was depleted, suggesting the NHR-23-depletion phenotype is independent from the insulin-signaling pathway (Fig. S4D).

To distinguish between larval arrest and developmental delay, we performed depletion experiments later in development where we could use vulval morphology to score progression through the L4 stage. We performed depletion experiments shifting early L3 animals onto auxin and monitored development by scoring vulva morphology 24 hours later. The majority of TIR1 animals developed to late L4, with auxin causing a slight developmental delay evidenced by more animals in mid-L4 (Fig. 3A,B). *nhr-23::AID*; *TIR1* animals grown on control plates also reached late L4 displaying the same slight developmental delay with a fraction of the population in mid-L4 (Fig. 3A,B). In contrast, when *nhr-23::AID*; *TIR1* animals were shifted to auxin, the vast majority of animals were early L4 larvae with a fraction of the population remaining in L3 (Fig. 3A,B). We repeated

these experiments, scoring *nhr-23::AID*; *TIR1* animals after 48 and 72 hours on auxin. After 48 hours a fraction of the population had reached mid-L4 and after 72 hours we observed adult animals as evidenced by the presence of oocytes (Fig. 3C,D). At both timepoints there was a subset of L4 larvae which we could not precisely stage due to aberrant vulval morphology (Fig. 3C,D); these animals had large vulval lumens reminiscent of a 4.3 stage vulva (Mok et al., 2015), but we also observed adults with a similar large vulval lumen (Fig. 3D). As animals progressed from 48 to 72 hours on auxin we saw an increasing fraction of dead animals which appeared necrotic with large fluid filled spaces within the animal (Fig. 3C,D). We then revisited our L1 depletion experiments, plating synchronized L1 larvae directly onto auxin plates and scoring animals 48 and 72 hours later. After 48 hours we observed animals with molting defects and necrosis, the fraction of which increased after 72 hours on auxin (Fig. 3E,F). Together, these data suggest that NHR-23 depletion causes developmental delay and animals die due to a failed molt.

**NHR-23 regulates oscillating genes involved in aECM biogenesis and regulation of protease activity**

To gain insight into how depletion of NHR-23 causes developmental delay, we analyzed the expression of NHR-23-regulated genes by mining existing microarray (Kouns et al., 2011) and oscillatory gene expression data (Hendriks et al., 2014)(Table S2). Of the 265 NHR-23 regulated genes, 236 (89%) were oscillatory (Table S2); a similar trend was observed in a recent analysis of these datasets (Tsiairis and Großhans, 2021). In contrast, 10-20% of *C. elegans* genes oscillate in expression (Hendriks et al., 2014; Kim et al., 2013; Meeuse et al., 2020)(Two-tailed Chi-squared test $p<0.0001$). To test whether these *nhr-23*-regulated oscillating genes were enriched for particular biological functions, we performed gene ontology analysis which indicated an enrichment in genes implicated in cuticle structure and regulation of endopeptidases (Table S3). These gene ontology classes are a specific subset of the functions enriched when we analyze all oscillating genes (Table S4). While the *C. elegans* genome encodes 181 collagen genes (Teuscher et al., 2019), *nhr-23* only regulated 13 collagens including all of the furrow collagens implicated in epidermal damage sensing (Table S2; *dpy-2, dpy-3, dpy-7, dpy-10*)(Dodd

et al., 2018). Other *nhr-23*-regulated collagens have well-described roles in body morphology (*sqt-1, sqt-2, rol-6*)(Kramer and Johnson, 1993). There are also several sets of genes involved in apical extracellular matrix biogenesis and remodeling, such as lipocalins, proteases, protease inhibitors, fibrillin, PAN and ZP domain-containing proteins, and leucine-rich repeat proteins. Although not enriched as a gene ontology class, NHR-23 also regulates several transcription factors implicated in molting or energy metabolism (*peb-1, nhr-91, dpy-20*)(Clark et al., 1995, 20; Fernandez et al., 2004; Kasuga et al., 2013). Most of the genes in these ontology classes have a peak phase following that of *nhr-23* (Fig. 4A,C).

To explore NHR-23 direct targets, we analyzed an NHR-23 L3 ChIP-seq dataset (Gerstein et al., 2010). As expected, NHR-23 was enriched in the promoter region of genes (Fig. 4B,S5). There was also notable enrichment downstream of the transcriptional end site (Fig. 4B,S6). We then examined whether NHR-23 was enriched near *nhr-23*-regulated oscillating genes. We converted the period to developmental time assuming a 9 hour larval stage which makes each hour equivalent to 40º. We separated the genes into three groups based on their peak phase. There were low levels of NHR-23 binding in genes that peaked in expression between 0 and 3 hours (Fig. 4B); *nhr-23* mRNA peaks at 178.11º/4.45 hours (Meeuse et al., 2020). In contrast, the genes that peaked in expression between 3 and 6 hours had much higher NHR-23 binding (Fig. 4B). The genes peaking in expression later (6-9 hours) had reduced NHR-23 binding, but still higher levels than the genes peaking between 0 and 3 hours (Fig. 4B). Thus genes which peak in expression close to when *nhr-23* mRNA levels peak tend to have higher NHR-23 levels upstream, downstream, and within their gene bodies (Fig. 4B).

As NHR-23-regulated oscillating genes were enriched in proteases and protease regulators (Table S2), we tested how NHR-23 depletion affected expression of a *nas-37* promoter reporter; *nas-37* is a protease implicated in *C. elegans* ecdysis (Davis et al., 2004). We released synchronized *nhr-23::AID, TIR1* animals carrying a *nas-37p::GFP::PEST* reporter onto control and auxin plates and monitored GFP expression over development. Animals growing on control media displayed oscillating reporter

activity with peaks at 18 and 30 hours (Fig. 5A,B). NHR-23 depleted animals exhibited a delayed onset of reporter expression and only a subset of animals expressed the reporter (Fig. 5A,B). There was only one pulse of *nas-37p::GFP::PEST* expression after which we detected no reporter activity (Fig. 5A,B). Together, these data confirm that NHR-23 regulates *nas-37* expression and that following NHR-23-depletion there is a weaker pulse of target gene expression followed by a failure to express again.

**NHR-23-depletion causes defects in aECM structure and function**

Defects in cuticle collagen patterns have been observed in *nas-37* mutants (Davis et al., 2004), so we examined whether NHR-23 depletion affected aECM structure. We used CRISPR/Cas9-mediated genome editing in *nhr-23::AID; TIR1* animals to introduce mNeonGreen (mNG)::3xFLAG cassettes into three genes in: i) *rol-6*; an intermediate collagen ii) *bli-1,* a collagen that forms struts in the adult cuticle; and iii) *noah-1*, a component of the transient sheath. *rol-6* and *noah-1* were regulated by *nhr-23* while *bli-1* is an adult-specific collagen expressed in L4 larvae, so would not be interrogated in the microarray experiment (Kouns et al., 2011). We first confirmed that each knock-in had a wild-type brood size (Fig S6A) and then tested fusion protein size by western blotting. Anti-FLAG immunoblotting on *nhr-23::AID; TIR1, rol-6::mNG::3xFLAG* lysates detected a single band of the expected size (~70 kDA; Fig S6B). In *noah-1::mNG::3xFLAG, nhr-23::AID; TIR1* lysates there was a band of the expected size (~150 kDa) as well as a lower ~50 kDa band. *noah-1* is only predicted to have a single isoform so this might reflect a cleavage or degradation product. In *nhr-23::AID; TIR1, bli-1::mNG::3xFLAG* there were several prominent bands smaller than the ~140 kDa predicted product (Fig S6C). These might reflect processing, which is common with collagens (Myllyharju and Kivirikko, 2004).

ROL-6 is a component of the L2, L3, L4 and adult cuticle. Expression in L1 larvae is first observed 14-16 hours post-release and subsequently is incorporated into annuli in the aECM (Fig. 6A). When we depleted NHR-23 in L3 larvae ROL-6::mNG expression appeared unaffected, but the annular localization was irregular and thicker and we observed gaps in the annular ROL-6::mNG over the seam cells (Fig. 6B). Many animals

had a corset of unshed cuticle to which ROL-6::mNG localized (Fig. 6C). We next addressed whether NHR-23 depletion affected the formation of struts in the cuticle medial layer. BLI-1 expression is first detected in hypodermal cells in stage 4.5 L4 larvae (Fig. 6D) where it also decorates annuli (Fig. 6E). It then becomes incorporated into struts by late L4 (Fig. 6F). We shifted *nhr-23::AID; TIR1, bli-1::mNG* animals onto control or auxin plates in early L3 and examined BLI-1::mNG expression and localization. We scored control animals after 24 hours on auxin when animals were late L4s and needed to score NHR-23 depleted animals 24 hours later due to the developmental delay. NHR-23 depletion caused reduced expression of BLI-1::mNG and a loss of the punctate pattern (Fig. 6F). BLI-1::mNG weakly localized to annuli and animals displayed bright, disorganized patches of BLI-1::mNG (Fig. 6F).

Based on the defects in ROL-6 and BLI-1 localization, we next examined whether NHR-23 depletion affected formation of the sheath, a transient pre-cuticular structure thought to play a role in patterning the cuticle (Cohen and Sundaram, 2020). NOAH-1 is a zona pellucida domain protein that is part of the pre-cuticular aECM in embryos and larvae. In L4 larvae, we observed the reported vulval lumenal localization and cuticular expression (Cohen et al., 2020), as well as localization to the rectum and excretory duct (Fig. 6G). NHR-23 depletion did not affect NOAH-1 localization in the excretory duct or rectum. Although vulval morphology is aberrant in NHR-23-depleted animals, NOAH-1 still localizes to cell surfaces (Fig. 6G). In mid-L4, NOAH-1 is normally localized to the cuticle and lysosomes and is absent from over the seam cells (Fig. 6G). NHR-23-depletion caused a loss of NOAH-1::mNG localization to annulli (Fig. 6G). Instead, we observed small irregular punctae and accumulation of NOAH-1::mNG over seam cells (Fig. 6G). Together, these data indicate that NHR-23 depletion leads to defective localization of proteins in both the collagenous cuticle and the sheath.

Given the defects in aECM structure following NHR-23-depletion, we tested whether the epidermal barrier was intact. First, we incubated control and auxin-treated *nhr-23::AID, TIR1* animals with the cuticle impermeable, cell membrane permeable Hoechst 33258 dye which stains nuclei. N2 and *TIR1* animals grown on control or auxin plates exhibited

low Hoechst staining in the head (4-15%) and body (0-0.7%). *nhr-23::AID, TIR1* animals grown on control plates exhibited higher head staining (40%) but no body staining, while almost all animals on auxin plates displayed Hoechst staining in their head and body (96% and 99%, respectively) (Fig. 7A). Animals shifted onto auxin early or late in L1 robustly expressed an *nlp-29p::GFP* reporter (Fig. 7B,C), which can be activated by infection, acute stress, and physical damage to the cuticle (Pujol et al., 2008; Zugasti and Ewbank, 2009). We further tested the cuticle integrity in a hypo-osmotic shock assay in which animals with defective cuticle barriers rapidly die following exposure to water (Kage-Nakadai et al., 2010). *TIR1* animals grown on control media or auxin were completely viable in water (Fig. 7D). *nhr-23::AID, TIR1* control animals had a weakly penetrant sensitivity to hypo-osmotic shock, while the same strain grown on auxin rapidly died following hypo-osmotic shock (Fig. 7D). These data suggest that NHR-23 is required for the cuticle barrier.

**_nhr-23_ is necessary in seam and hypodermal cells for larval development**

Finally, we wished to determine in which cells *nhr-23* was necessary for larval development through a tissue-specific RNAi approach. In RNAi-proficient N2 animals, 100% of *nhr-23(RNAi)* animals exhibited developmental delay and molting defects (Fig. 8A-C). *nhr-23* knockdown in body-wall muscle and intestinal cells produced no molting defects and we observed only mild developmental delay (0-11.5% of animals)(Fig. 8A-C). Vulval precursor cell-specific *nhr-23(RNAi)* caused molting defects in 23.4% of animals and we also observed developmental delay in 22.1% of animals. We observed highly penetrant developmental delay (90.4%) and molting defects (39.9%) when we performed *nhr-23* RNAi in a strain using a *wrt-2* promoter for tissue-specific RNAi (Fig. 8A-C). *wrt-2* is expressed in seam cells, rectal cells and hypodermal cells (Fig. S7C,D; Aspöck et al., 1999). Given this result and the defective ROL-6::mNG and NOAH-1::mNG (Fig. 6) localization over seam cells, we generated more tissue-restricted RNAi strains. We used a minimal seam cell-specific enhancer with a *pes-10* minimal promoter (Ashley et al., 2021), which is robustly expressed in seam cells with some weak hypodermal expression (Fig. S7A,B). To test the specificity of this strain, we introduced a *his-72::mNG* knock-in. In control animals, we observed nuclear expression in seam, hypodermal,

intestinal, vulval and germline cells, as expected for a histon H3 fusion (Fig S8). *mNeonGreen* RNAi caused reduced HIS-72::mNG expression in seam, hypodermal syncytium, and intestinal nuclei. *nhr-23(RNAi)* in the *SCMp* RNAi strain phenocopied *nhr-23(RNAi*) in N2 animals with almost all animals exhibiting developmental delay (99.3%) and molting defects (98.7%)(Fig. 8A-C). Notably, intestine-specific *nhr-23* RNAi did not cause phenotypes (Fig. 8A-C). We then constructed a hypodermis-specific RNAi strain using the *semo-1* promoter (Kaletsky et al., 2018; Köhnlein et al., 2020). *nhr-23* RNAi in this strain produced molting defects and developmental delay, though with less penetrance compared to our *SCMp*-specific RNAi strain (Fig 8A-C). To test the effect of *SCMp*-specific *nhr-23* knockdown on the aECM, we introduced a BLI-1::mNG knock-ins in our seam cell-specific RNAi strain. *nhr-23* depletion in this strain caused reduced BLI-1 levels, similar to NHR-23 protein depletion in the soma (Figs. 6F, 8D). BLI-1::mNG also was observed over the seam cells, which does not occur in wild-type animals (Fig. 8D). Together these data indicated that *nhr-23* is necessary in the seam and hypodermal cells for timely developmental progression, completion of molting, and aECM formation.

## DISCUSSION

*C. elegans* molting is a powerful system to understand developmentally programmed aECM regeneration. In this study**,** we determine when and where NHR-23 acts and how it promotes aECM regeneration. NHR-23 oscillates and depletion early in L1 larvae causes severe developmental delay. NHR-23-depletion in L3 larvae causes a similar delay during the L4 stage. *nhr-23*-regulated genes are enriched for cuticle components and protease inhibitors, and NHR-23 is enriched at the transcription start and end sites of target genes. NHR-23-depletion causes aberrant localization of the early collagen ROL-6 and the pre-cuticle component, NOAH-1. It also causes severely reduced levels of the medial layer collagen BLI-1, which is also mislocalized. These cuticle defects are correlated with a loss of the cuticle barrier. Tissue-specific RNAi suggested that *nhr-23* is necessary in seam and hypodermal cells.

### NHR-23 is necessary for cuticle structure and function

Integration of *nhr-23(RNAi)* microarray and NHR-23 ChIP-seq datasets suggests that NHR-23 regulates a set of pre-cuticle, early collagen, protease inhibitor genes (Gerstein et al., 2010; Kouns et al., 2011). NHR-23 binds more robustly in the promoter and transcription end site of genes which peak in expression closer to the *nhr-23* mRNA peak in expression (Fig. 4). One intriguing possibility is that the earlier NHR-23-regulated genes may be more sensitive to NHR-23 levels. This model would align with *E. coli* amino acid biosynthesis gene regulation where enzymes earlier in the pathway have more responsive promoters with higher activity (Zaslaver et al., 2004). We validated that NHR-23 regulates the expression of *nas-37*, a protease implicated in molting (Fig. 5). Curiously, two other targets (*noah-1, rol-6*) seemed to be expressed at near wild-type levels, but displayed aberrant localization (Fig. 6). These data highlight a potential limitation of a single time point gene expression study. A shift in phase of an oscillating gene without change in amplitude could create the appearance of up- or down-regulation depending on the sampling time point (Tsiairis and Großhans, 2021). The *nhr-23(RNAi)* microarray is a useful starting point to understand how NHR-23 promotes molting, but an RNA-seq time course on NHR-23 depleted animals may be necessary to identify regulated genes. Such an approach was necessary to determine how the pioneer factor, BLMP-1, promotes developmental timing (Hauser et al., 2021).

NHR-23-depletion caused aberrant localization of NOAH-1 and ROL-6, lower levels of BLI-1 (Fig. 6) and a severe barrier defect (Fig. 7). There are numerous *nhr-23*-regulated genes which are implicated in the epithelial barrier. The cuticle furrow formed by six *nhr-23*-regulated collagens (*dpy-2, dpy-3, dpy-7, dpy-8, dpy-9, dpy-10*) is thought to be monitored by a sensor which coordinates a number of stress responses following detection (Dodd et al., 2018). An RNAi screen of 91 collagens found that inactivation of only these six collagens caused a barrier defect (Sandhu et al., 2021). Inactivation of a subset of the furrow collagens causes permeability to Hoechst 33458 dye and elevated *nlp-29p::GFP* reporter activity (Dodd et al., 2018), consistent with our NHR-23-depletion data (Fig. 7). *bus-8* is a predicted glycosyltransferase that plays a role in the epithelial barrier and is also *nhr-23*-regulated and its peak expression follows that of the furrow collagens (Table S1). Screening *nhr-23* regulated genes may find other genes implicated

in the epithelial barrier and the peak phase could provide insight into how this barrier is constructed.

**NHR-23 acts in seam and hypodermal cells to promote molting**

When we depleted NHR-23 early in L1, animals appeared wild type with few molting defects, whereas later depletion produced strong molting defects (Fig. 2). This difference in phenotypes reflected severe developmental delay when we depleted NHR-23 early in L1. A similar result was observed when we depleted NHR-23 in L3 larvae; it took an extra 48 hours for animals to reach late L4 or early adulthood (Fig. 3). This observation is consistent with RNAi data demonstrating that *nhr-23* knockdown causes developmental delay, while overexpression accelerates development (Macneil et al., 2013; Meeuse et al., 2022). An NHR-23-regulated promoter reporter (*nas-37p::GFP::PEST*) peaked at a similar time in control and NHR-23-depleted animals (Fig. 5), but was expressed at lower levels. This data might suggest that the low levels of NHR-23 present are sufficient to drive low levels of target gene expression. An interesting future question is what is driving NHR-23-depleted animals to eventually attempt to molt? The pre-cuticle component, NOAH-1, and early collagen, ROL-6 are both expressed and secreted but display localization defects. One possibility is that low sustained NHR-23-levels eventually allow the accumulation of factors that initiate apolysis but there is insufficient expression. *nas-37* is necessary for *C. elegans* ecdysis and recombinant NAS-37 promotes the formation of retractile rings, a structure associated with molting, in the parasitic nematode *H. contortus* (Davis et al., 2004). Another non-exclusionary possibility is that NHR-23 controls the expression of transcription factors in a regulatory cascade, similar to the gene regulatory network controlling insect molting (King-Jones and Thummel, 2005; Thummel, 1990). *nhr-23* regulates *peb-1* and *dpy-20*, transcription factors with known roles in molting (Clark et al., 1995, 20; Fernandez et al., 2004, 1). *nhr-23* also regulates *nhr-91* (Kouns et al., 2011)(Table S2), a nuclear hormone receptor involved in blast cell progression in response to nutrients (Kasuga et al., 2013). A third possibility is that another timer eventually promotes molting. The molting timer and heterochronic cycles can be uncoupled, causing animals to attempt molting before completion of cell division and differentiation, leading to death (Ruaud and Bessereau, 2006).

### *nhr-23* is necessary in seam and hypodermal cells to promote molting

When we performed *SCMp*-specific *nhr-23* RNAi, we observed severe developmental delay and molting defects (Fig 8). Hypodermal-specific *nhr-23* knock-down produced less penetrant phenotypes (Fig. 8). The most severe defects in ROL-6 and NOAH-1 localization occur above the seam cells (Figure 6). This observation combined with the tissue-specific RNAi data suggests that NHR-23 may be necessary in seam cells for molting, though we cannot rule out an additional role in the hypodermis. However, we observed reduced expression and patchy cuticular localization following NHR-23 depletion (Fig. 6), suggesting either that NHR-23 functions in the hypodermis to regulate BLI-1 expression or it is acting cell non-autonomously in the seam cells. Determining how NHR-23 regulates BLI-1 expression and formation of struts will provide insight into aECM assembly. *nhr-23* is expressed in other epidermal cells that produce pre-cuticle and cuticle, such as vulval precursor cells, rectal cells, and excretory duct cells. NHR-23 depletion did not produce obvious defects in localization of the pre-cuticle component NOAH-1 in these cells (Fig 6). We did not see phenotypes such as excretory duct or pore lumen dilations, which would be indicative of excretory system defects (Gill et al., 2016). We observed vulval morphology defects following NHR-23 depletion, but it is not clear whether that is due to NHR-23 regulation of this specialized aECM or if it is the consequence of developmental delay and failure to molt. Tissue-specific RNAi or protein depletion will be required to determine whether NHR-23 activity is necessary in these epithelial cells, or if it predominantly functions in seam and hypodermal cells.

### Future perspectives

This work highlights the power of timed protein depletion for dissecting the role of oscillating developmental regulators in development. As transcription factors coordinate the expression of batteries of genes in a given biological process, future work will reveal how NHR-23 coordinates apical ECM remodeling, apolysis, and ecdysis. NHR-23 oscillates in the soma yet is constitutively expressed in the germline (Ragle et al., 2020). Exploring the differences between oscillatory and constitutive NHR-23 expression could shed light on mammalian gene regulation, as several circadian rhythm regulators oscillate

in the soma but are constitutively expressed in the testes (Alvarez et al., 2008; Kang et al., 2010; Kennaway et al., 2012; Morse et al., 2003).

## References


**Agbulut, O., Coirault, C., Niederländer, N., Huet, A., Vicart, P., Hagège, A., Puceat, M. and Menasché, P.** (2006). GFP expression in muscle cells impairs actin-myosin interactions: implications for cell therapy. *Nat. Methods* **3**, 331–331.

**Alvarez, J. D., Hansen, A., Ord, T., Bebas, P., Chappell, P. E., Giebultowicz, J. M., Williams, C., Moss, S. and Sehgal, A.** (2008). The circadian clock protein BMAL1 is necessary for fertility and proper testosterone production in mice. *J. Biol. Rhythms* **23**, 26–36.

**Antebi, A.** (2015). Nuclear receptor signal transduction in *C. elegans*. *WormBook* 1–49.

**Ashley, G. E., Duong, T., Levenson, M. T., Martinez, M. A. Q., Johnson, L. C., Hibshman, J. D., Saeger, H. N., Palmisano, N. J., Doonan, R., Martinez-Mendez, R., et al.** (2021). An expanded auxin-inducible degron toolkit for *Caenorhabditis elegans*. *Genetics* **217**, iyab006.

**Aspöck, G., Kagoshima, H., Niklaus, G. and Bürglin, T. R.** (1999). *Caenorhabditis elegans* has scores of hedgehog-related genes: sequence and expression analysis. *Genome Res.* **9**, 909–923.

**Baens, M., Noels, H., Broeckx, V., Hagens, S., Fevery, S., Billiau, A. D., Vankelecom, H. and Marynen, P.** (2006). The Dark Side of EGFP: Defective Polyubiquitination. *PLOS ONE* **1**, e54.

**Barkoulas, M., van Zon, J. S., Milloz, J., Van Oudenaarden, A. and Félix, M.-A.** (2013). Robustness and Epistasis in the *C. elegans* Vulval Signaling Network Revealed by Pathway Dosage Modulation. *Dev. Cell* **24**, 64–75.

**Baugh, L. R. and Sternberg, P. W.** (2006). DAF-16/FOXO regulates transcription of *cki-1*/Cip/Kip and repression of *lin-4* during *C. elegans* L1 arrest. *Curr. Biol.* **16**, 780–785.

**Blaxter, M. L.** (1993). Cuticle surface proteins of wild type and mutant *Caenorhabditis elegans*. *J. Biol. Chem.* **268**, 6600–6609.

**Blaxter, M. L., Page, A. P., Rudin, W. and Maizels, R. M.** (1992). Nematode surface coats: actively evading immunity. *Parasitol. Today Pers. Ed* **8**, 243–247.

**Brenner, S.** (1974). The genetics of *Caenorhabditis elegans*. *Genetics* **77**, 71–94.

**Bridgham, J. T., Eick, G. N., Larroux, C., Deshpande, K., Harms, M. J., Gauthier, M. E. A., Ortlund, E. A., Degnan, B. M. and Thornton, J. W.** (2010). Protein Evolution by Molecular Tinkering: Diversification of the Nuclear Receptor Superfamily from a Ligand-Dependent Ancestor. *PLoS Biol.* **8**, e1000497.

**Campbell, L. A., Faivre, E. J., Show, M. D., Ingraham, J. G., Flinders, J., Gross, J. D. and Ingraham, H. A.** (2008). Decreased Recognition of SUMO-Sensitive Target Genes following Modification of SF-1 (NR5A1). *Mol. Cell. Biol.* **28**, 7476–7486.

**Church, D. L., Guan, K. L. and Lambie, E. J.** (1995). Three genes of the MAP kinase cascade, *mek-2*, *mpk-1/sur-1* and *let-60 ras*, are required for meiotic cell cycle progression in *Caenorhabditis elegans*. *Development* **121**, 2525–2535.

**Clark, D. V., Suleman, D. S., Beckenbach, K. A., Gilchrist, E. J. and Baillie, D. L.** (1995). Molecular cloning and characterization of the *dpy-20* gene of *Caenorhabditis elegans*. *Mol. Gen. Genet. MGG* **247**, 367–378.

**Cohen, J. D. and Sundaram, M. V.** (2020). *C. elegans* Apical Extracellular Matrices Shape Epithelia. *J. Dev. Biol.* **8**, 23.

**Cohen, J. D., Sparacio, A. P., Belfi, A. C., Forman-Rubinsky, R., Hall, D. H., Maul-Newby, H., Frand, A. R. and Sundaram, M. V.** (2020). A multi-layered and dynamic apical extracellular matrix shapes the vulva lumen in *Caenorhabditis elegans*. *eLife* **9**, e57874.

**Davis, M. W., Birnie, A. J., Chan, A. C., Page, A. P. and Jorgensen, E. M.** (2004). A conserved metalloprotease mediates ecdysis in *Caenorhabditis elegans*. *Development* **131**, 6001–6008.

**de Sousa Abreu, R., Penalva, L. O., Marcotte, E. M. and Vogel, C.** (2009). Global signatures of protein and mRNA expression levels. *Mol. Biosyst.* **5**, 1512–1526.

**Dodd, W., Tang, L., Lone, J.-C., Wimberly, K., Wu, C.-W., Consalvo, C., Wright, J. E., Pujol, N. and Choe, K. P.** (2018). A Damage Sensor Associated with the Cuticle Coordinates Three Core Environmental Stress Responses in

*Caenorhabditis elegans*. *Genetics* **208**, 1467–1482.

**Eick, G. N. and Thornton, J. W.** (2011). Evolution of steroid receptors from an estrogen-sensitive ancestral receptor. *Mol. Cell. Endocrinol.* **334**, 31–38.

**Espelt, M. V., Estevez, A. Y., Yin, X. and Strange, K.** (2005). Oscillatory Ca2+ signaling in the isolated *Caenorhabditis elegans* intestine: role of the inositol-1,4,5-trisphosphate receptor and phospholipases C beta and gamma. *J. Gen. Physiol.* **126**, 379–392.

**Fernandez, A. P., Gibbons, J. and Okkema, P. G.** (2004). *C. elegans peb-1* mutants exhibit pleiotropic defects in molting, feeding, and morphology. *Dev. Biol.* **276**, 352–366.

**Fielenbach, N. and Antebi, A.** (2008). *C. elegans* dauer formation and the molecular basis of plasticity. *Genes Dev.* **22**, 2149–2165.

**Forman-Rubinsky, R., Cohen, J. D. and Sundaram, M. V.** (2017). Lipocalins Are Required for Apical Extracellular Matrix Organization and Remodeling in *Caenorhabditis elegans*. *Genetics* **207**, 625–642.

**Frand, A. R., Russel, S. and Ruvkun, G.** (2005). Functional Genomic Analysis of *C. elegans* Molting. *PLoS Biol.* **3**, e312.

**Frøkjaer-Jensen, C., Davis, M. W., Hopkins, C. E., Newman, B. J., Thummel, J. M., Olesen, S.-P., Grunnet, M. and Jorgensen, E. M.** (2008). Single-copy insertion of transgenes in *Caenorhabditis elegans*. *Nat. Genet.* **40**, 1375–1383.

**Gerstein, M. B., Lu, Z. J., Van Nostrand, E. L., Cheng, C., Arshinoff, B. I., Liu, T., Yip, K. Y., Robilotto, R., Rechtsteiner, A., Ikegami, K., et al.** (2010). Integrative Analysis of the *Caenorhabditis elegans* Genome by the modENCODE Project. *Sci. N. Y. NY* **330**, 1775–1787.

**Ghanta, K. S. and Mello, C. C.** (2020). Melting dsDNA Donor Molecules Greatly Improves Precision Genome Editing in *Caenorhabditis elegans*. *Genetics* **216**, 643–650.

**Ghedin, E., Wang, S., Spiro, D., Caler, E., Zhao, Q., Crabtree, J., Allen, J. E., Delcher, A. L., Guiliano, D. B., Miranda-Saavedra, D., et al.** (2007). Draft genome of the filarial nematode parasite *Brugia malayi*. *Science* **317**, 1756–1760.

**Gibson, D. G., Young, L., Chuang, R.-Y., Venter, J. C., Hutchison, C. A. and Smith, H. O.** (2009). Enzymatic assembly of DNA molecules up to several hundred kilobases. *Nat. Methods* **6**, 343–345.

**Gill, H. K., Cohen, J. D., Ayala-Figueroa, J., Forman-Rubinsky, R., Poggioli, C., Bickard, K., Parry, J. M., Pu, P., Hall, D. H. and Sundaram, M. V.** (2016). Integrity of Narrow Epithelial Tubes in the C. elegans Excretory System Requires a Transient Luminal Matrix. *PLoS Genet.* **12**, e1006205.

**Gissendanner, C. R., Crossgrove, K., Kraus, K. A., Maina, C. V. and Sluder, A. E.** (2004). Expression and function of conserved nuclear receptor genes in *Caenorhabditis elegans*. *Dev. Biol.* **266**, 399–416.

**Harfe, B. D., Gomes, A. V., Kenyon, C., Liu, J., Krause, M. and Fire, A.** (1998). Analysis of a *Caenorhabditis elegans* Twist homolog identifies conserved and divergent aspects of mesodermal patterning. *Genes Dev.* **12**, 2623–2635.

**Hauser, Y. P., Meeuse, M. W. M., Gaidatzis, D. and Großhans, H.** (2021). The BLMP-1 transcription factor promotes oscillatory gene expression to achieve timely molting. *bioRxiv* 2021.07.05.450828.

**Hendriks, G.-J., Gaidatzis, D., Aeschimann, F. and Großhans, H.** (2014). Extensive oscillatory gene expression during *C. elegans* larval development. *Mol. Cell* **53**, 380–392.

**Huber, W., Carey, V. J., Gentleman, R., Anders, S., Carlson, M., Carvalho, B. S., Bravo, H. C., Davis, S., Gatto, L., Girke, T., et al.** (2015). Orchestrating high-throughput genomic analysis with Bioconductor. *Nat. Methods* **12**, 115–121.

**Jetten, A. M.** (2009). Retinoid-related orphan receptors (RORs): critical roles in development, immunity, circadian rhythm, and cellular metabolism. *Nucl. Recept. Signal.* **7**,.

**Johnstone, I. L. and Barry, J. D.** (1996). Temporal reiteration of a precise gene expression pattern during nematode development. *EMBO J.* **15**, 3633–3639.

**Kage-Nakadai, E., Kobuna, H., Kimura, M., Gengyo-Ando, K., Inoue, T., Arai, H. and Mitani, S.** (2010). Two very long chain fatty acid acyl-CoA synthetase genes, *acs-20* and *acs-22*, have roles in the cuticle surface barrier in *Caenorhabditis elegans*. *PLoS ONE* **5**, e8857.

**Kaletsky, R., Yao, V., Williams, A., Runnels, A. M., Tadych, A., Zhou, S., Troyanskaya, O. G. and Murphy, C. T.** (2018). Transcriptome analysis of adult *Caenorhabditis elegans* cells reveals tissue-specific gene and isoform expression. *PLOS Genet.* **14**, e1007559.

**Kang, T.-H., Lindsey-Boltz, L. A., Reardon, J. T. and Sancar, A.** (2010). Circadian control of XPA and excision repair of cisplatin-DNA damage by cryptochrome and HERC2 ubiquitin ligase. *Proc. Natl. Acad. Sci.* **107**, 4890–4895.

**Kaplan, R. E. W. and Baugh, L. R.** (2016). L1 arrest, *daf-16*/FoxO and nonautonomous control of post-embryonic development. *Worm* **5**, e1175196.

**Kasuga, H., Fukuyama, M., Kitazawa, A., Kontani, K. and Katada, T.** (2013). The microRNA miR-235 couples blast-cell quiescence to the nutritional state. *Nature* **497**, 503–506.

**Kelley, M., Yochem, J., Krieg, M., Calixto, A., Heiman, M. G., Kuzmanov, A., Meli, V., Chalfie, M., Goodman, M. B., Shaham, S., et al.** (2015). FBN-1, a fibrillin-related protein, is required for resistance of the epidermis to mechanical deformation during *C. elegans* embryogenesis. *eLife* **4**, 1629.

**Kennaway, D. J., Boden, M. J. and Varcoe, T. J.** (2012). Circadian rhythms and fertility. *Mol. Cell. Endocrinol.* **349**, 56–61.

**Kim, D. hyun, Grün, D. and van Oudenaarden, A.** (2013). Dampening of expression oscillations by synchronous regulation of a microRNA and its target. *Nat. Genet.* **45**, 1337–1344.

**King-Jones, K. and Thummel, C. S.** (2005). Nuclear receptors-a perspective from *Drosophila*. *Nat. Rev. Genet.* **6**, 311–323.

**Köhnlein, K., Urban, N., Guerrero-Gómez, D., Steinbrenner, H., Urbánek, P., Priebs, J., Koch, P., Kaether, C., Miranda-Vizuete, A. and Klotz, L.-O.** (2020). A *Caenorhabditis elegans* ortholog of human selenium-binding protein 1 is a pro-aging factor protecting against selenite toxicity. *Redox Biol.* **28**, 101323.

**Kostrouchova, M., Krause, M., Kostrouch, Z. and Rall, J. E.** (1998). CHR3: a *Caenorhabditis elegans* orphan nuclear hormone receptor required for proper epidermal development and molting. *Development* **125**, 1617–1626.

**Kostrouchova, M., Krause, M., Kostrouch, Z. and Rall, J. E.** (2001). Nuclear

hormone receptor CHR3 is a critical regulator of all four larval molts of the nematode *Caenorhabditis elegans*. *Proc. Natl. Acad. Sci. U. S. A.* **98**, 7360–7365.

**Kouns, N. A., Nakielna, J., Behensky, F., Krause, M. W., Kostrouch, Z. and Kostrouchova, M.** (2011). NHR-23 dependent collagen and hedgehog-related genes required for molting. *Biochem. Biophys. Res. Commun.* **413**, 515–520.

**Kramer, J. M. and Johnson, J. J.** (1993). Analysis of mutations in the sqt-1 and rol-6 collagen genes of Caenorhabditis elegans. *Genetics* **135**, 1035–1045.

**Lam, G. T., Jiang, C. and Thummel, C. S.** (1997). Coordination of larval and prepupal gene expression by the DHR3 orphan receptor during *Drosophila* metamorphosis. *Development* **124**, 1757–1769.

**Lažetić, V. and Fay, D. S.** (2017). Molting in *C. elegans*. *Worm* **6**, 1–20.

**Lin, K., Dorman, J. B., Rodan, A. and Kenyon, C.** (1997). *daf-16*: An HNF-3/forkhead family member that can function to double the life-span of *Caenorhabditis elegans*. *Science* **278**, 1319–1322.

**Macneil, L. T., Watson, E., Arda, H. E., Zhu, L. J. and Walhout, A. J. M.** (2013). Diet-Induced Developmental Acceleration Independent of TOR and Insulin in *C. elegans*. *Cell* **153**, 240–252.

**Meeuse, M. W., Hauser, Y. P., Morales Moya, L. J., Hendriks, G., Eglinger, J., Bogaarts, G., Tsiairis, C. and Großhans, H.** (2020). Developmental function and state transitions of a gene expression oscillator in *Caenorhabditis elegans*. *Mol. Syst. Biol.* **16**,.

**Meeuse, M. W. M., Nahar, S., Braun, K. and Großhans, H.** (2022). The Grainyhead/LSF transcription factor GRH-1 is rhythmically required for molting. 2022.03.01.482504.

**Mello, C. C., Kramer, J. M., Stinchcomb, D. and Ambros, V.** (1991). Efficient gene transfer in *C. elegans*: extrachromosomal maintenance and integration of transforming sequences. *EMBO J.* **10**, 3959–3970.

**Melo, J. A. and Ruvkun, G.** (2012). Inactivation of conserved *C. elegans* genes engages pathogen- and xenobiotic-associated defenses. *Cell* **149**, 452–466.

**Mok, D. Z. L., Sternberg, P. W. and Inoue, T.** (2015). Morphologically defined sub-

stages of *C. elegans* vulval development in the fourth larval stage. *BMC Dev. Biol.* 1–8.

**Moribe, H., Yochem, J., Yamada, H., Tabuse, Y., Fujimoto, T. and Mekada, E.** (2004). Tetraspanin protein (TSP-15) is required for epidermal integrity in *Caenorhabditis elegans*. *J. Cell Sci.* **117**, 5209–5220.

**Morse, D., Cermakian, N., Brancorsini, S., Parvinen, M. and Sassone-Corsi, P.** (2003). No circadian rhythms in testis: Period1 expression is clock independent and developmentally regulated in the mouse. *Mol. Endocrinol.* **17**, 141–151.

**Myllyharju, J. and Kivirikko, K. I.** (2004). Collagens, modifying enzymes and their mutations in humans, flies and worms. *Trends Genet. TIG* **20**, 33–43.

**Nelson, F. K., Albert, P. S. and Riddle, D. L.** (1983). Fine structure of the *Caenorhabditis elegans secretory-excretory system*. *J. Ultrastruct. Res.* **82**, 156–171.

**Nonet, M. L.** (2020). Efficient Transgenesis in *Caenorhabditis elegans* Using Flp Recombinase-Mediated Cassette Exchange. *Genetics* **215**, 903–921.

**Page, A. P. and Johnstone, I. L.** (2007). The cuticle. *WormBook Online Rev. C Elegans Biol.* 1–15.

**Paix, A., Wang, Y., Smith, H. E., Lee, C.-Y. S., Calidas, D., Lu, T., Smith, J., Schmidt, H., Krause, M. W. and Seydoux, G.** (2014). Scalable and versatile genome editing using linear DNAs with microhomology to Cas9 Sites in *Caenorhabditis elegans*. *Genetics* **198**, 1347–1356.

**Paix, A., Folkmann, A., Rasoloson, D. and Seydoux, G.** (2015). High Efficiency, Homology-Directed Genome Editing in *Caenorhabditis elegans* Using CRISPR-Cas9 Ribonucleoprotein Complexes. *Genetics* **201**, 47–54.

**Posch, A., Kohn, J., Oh, K., Hammond, M. and Liu, N.** (2013). V3 stain-free workflow for a practical, convenient, and reliable total protein loading control in western blotting. *J. Vis. Exp.* 50948.

**Pujol, N., Cypowyj, S., Ziegler, K., Millet, A., Astrain, A., Goncharov, A., Jin, Y., Chisholm, A. D. and Ewbank, J. J.** (2008). Distinct innate immune responses to infection and wounding in the *C. elegans* epidermis. *Curr. Biol.* **18**, 481–489.

**R Core Team** *R: A language and environment for statistical computing.* Vienna,

Austria: R Foundation for Statistical Computing.

**Ragle, J. M., Aita, A. L., Morrison, K. N., Martinez-Mendez, R., Saeger, H. N., Ashley, G. A., Johnson, L. C., Schubert, K. A., Shakes, D. C. and Ward, J. D.** (2020). The conserved molting/circadian rhythm regulator NHR-23/NR1F1 serves as an essential co-regulator of *C. elegans* spermatogenesis. *Development* **147**, dev193862.

**Roach, N. P., Sadowski, N., Alessi, A. F., Timp, W., Taylor, J. and Kim, J. K.** (2020). The full-length transcriptome of *C. elegans* using direct RNA sequencing. *Genome Res.*

**Ruaud, A.-F. and Bessereau, J.-L.** (2006). Activation of nicotinic receptors uncouples a developmental timer from the molting timer in *C. elegans*. *Development* **133**, 2211–2222.

**Ruaud, A.-F., Lam, G. and Thummel, C. S.** (2010). The *Drosophila* nuclear receptors DHR3 and FTZ-F1 control overlapping developmental responses in late embryos. *Development* **137**, 123–131.

**Sandhu, A., Badal, D., Sheokand, R., Tyagi, S. and Singh, V.** (2021). Specific collagens maintain the cuticle permeability barrier in *Caenorhabditis elegans*. *Genetics* **217**,.

**Sapio, M. R., Hilliard, M. A., Cermola, M., Favre, R. and Bazzicalupo, P.** (2005). The Zona Pellucida domain containing proteins, CUT-1, CUT-3 and CUT-5, play essential roles in the development of the larval alae in *Caenorhabditis elegans*. *Dev. Biol.* **282**, 231–245.

**Schindler, A. J., Baugh, L. R. and Sherwood, D. R.** (2014). Identification of Late Larval Stage Developmental Checkpoints in *Caenorhabditis elegans* Regulated by Insulin/IGF and Steroid Hormone Signaling Pathways. *PLoS Genet.* **10**, e1004426.

**Singh, R. N. and Sulston, J. E.** (1978). Some observations on molting in *C. elegans*. *Nematologica* **24**, 63–71.

**Stempor, P. and Ahringer, J.** (2016). SeqPlots - Interactive software for exploratory data analyses, pattern discovery and visualization in genomics. *Wellcome Open Res.* **1**, 14.

**Sulston, J. E. and Horvitz, H. R.** (1977). Post-embryonic cell lineages of the nematode, *Caenorhabditis elegans*. *Dev. Biol.* **56**, 110–156.

**Tabara, H., Sarkissian, M., Kelly, W. G., Fleenor, J., Grishok, A., Timmons, L., Fire, A. and Mello, C. C.** (1999). The *rde-1* gene, RNA interference, and transposon silencing in *C. elegans*. *Cell* **99**, 123–132.

**Taubert, S., Ward, J. D. and Yamamoto, K. R.** (2011). Nuclear hormone receptors in nematodes: Evolution and function. *Mol. Cell. Endocrinol.* **334**, 49–55.

**Telford, M. J., Bourlat, S. J., Economou, A., Papillon, D. and Rota-Stabelli, O.** (2008). The evolution of the Ecdysozoa. *Philos. Trans. R. Soc. B Biol. Sci.* **363**, 1529–1537.

**Teuscher, A. C., Jongsma, E., Davis, M. N., Statzer, C., Gebauer, J. M., Naba, A. and Ewald, C. Y.** (2019). The *in-silico* characterization of the *Caenorhabditis elegans* matrisome and proposal of a novel collagen classification. *Matrix Biol. Plus* **1**, 100001.

**Thummel, C. S.** (1990). Puffs and gene regulation-molecular insights into the *Drosophila* ecdysone regulatory hierarchy. *BioEssays News Rev. Mol. Cell. Dev. Biol.* **12**, 561–568.

**Tsiairis, C. and Großhans, H.** (2021). Chapter Two - Gene expression oscillations in *C. elegans* underlie a new developmental clock. In *Current Topics in Developmental Biology* (ed. Jarriault, S. and Podbilewicz, B.), pp. 19–43. Academic Press.

**Vo, A. A., Levenson, M. T., Ragle, J. M. and Ward, J. D.** (2021). Efficient generation of a single-copy *eft-3p::TIR1::F2A:: BFP::AID*::NLS* allele in the *C. elegans ttTi5605* insertion site through recombination-mediated cassette exchange. *MicroPublication Biol.* **2021**,.

**Vogel, C. and Marcotte, E. M.** (2012). Insights into the regulation of protein abundance from proteomic and transcriptomic analyses. *Nat. Rev. Genet.* **13**, 227–232.

**Vuong-Brender, T. T. K., Suman, S. K. and Labouesse, M.** (2017). The apical ECM preserves embryonic integrity and distributes mechanical stress during morphogenesis. *Development* **144**, 4336–4349.

**Ward, J. D.** (2015a). Rapid and Precise Engineering of the *Caenorhabditis elegans*

Genome with Lethal Mutation Co-Conversion and Inactivation of NHEJ Repair. *Genetics* **199**, 363–377.

**Ward, J. D.** (2015b). Rendering the Intractable More Tractable: Tools from *Caenorhabditis elegans* Ripe for Import into Parasitic Nematodes. *Genetics* **201**, 1279–1294.

**Ward, J. D., Bojanala, N., Bernal, T., Ashrafi, K., Asahina, M. and Yamamoto, K. R.** (2013). Sumoylated NHR-25/NR5A Regulates Cell Fate during *C. elegans* Vulval Development. *PLoS Genet.* **9**, e1003992.

**Ward, J. D., Mullaney, B., Schiller, B. J., He, L. D., Petnic, S. E., Couillault, C., Pujol, N., Bernal, T. U., Van Gilst, M. R., Ashrafi, K., et al.** (2014). Defects in the *C. elegans* acyl-CoA Synthase, *acs-3*, and Nuclear Hormone Receptor, *nhr-25*, Cause Sensitivity to Distinct, but Overlapping Stresses. *PLoS ONE* **9**, e92552.

**Watts, J. S., Harrison, H. F., Omi, S., Guenthers, Q., Dalelio, J., Pujol, N. and Watts, J. L.** (2020). New Strains for Tissue-Specific RNAi Studies in *Caenorhabditis elegans*. *G3 Bethesda Md* **10**, 4167–4176.

**Zaslaver, A., Mayo, A. E., Rosenberg, R., Bashkin, P., Sberro, H., Tsalyuk, M., Surette, M. G. and Alon, U.** (2004). Just-in-time transcription program in metabolic pathways. *Nat. Genet.* **36**, 486–491.

**Zhang, L., Ward, J. D., Cheng, Z. and Dernburg, A. F.** (2015). The auxin-inducible degradation (AID) system enables versatile conditional protein depletion in *C. elegans*. *Development* **142**, 4374–4384.

**Zugasti, O. and Ewbank, J. J.** (2009). Neuroimmune regulation of antimicrobial peptide expression by a noncanonical TGF-β signaling pathway in *Caenorhabditis elegans* epidermis. *Nat. Immunol.* **10**, 249–256.

## FIGURE LEGENDS

**Fig. 1. NHR-23 protein oscillates during development.** (A) A schematic of *nhr-23* mRNA expression across *C.* elegans larval development created with BioRender.com. The relative abundance of mRNA is based on the qRT-PCR analysis by Gissendanner et al., 2004. (B) Representative images from a time course monitoring the expression of

endogenous NHR-23 protein over the first 28 hours of larval development. The appropriate timing of the L1/L2 and L2/L3 molts is indicated. *nhr-23::GFP::AID*::3xFLAG* (B) and *nhr-23::AID*::3xFLAG* (C) are previously described endogenous knock-ins that produce C-terminal translational fusions to all known *nhr-23* isoforms (Ragle et al., 2020; Zhang et al., 2015). Two biological replicates were performed and the number of animals for which the image is representative at each timepoint is provided. Scale bars=20 µm. (C) Anti-FLAG immunoblot analysis of synchronized *nhr-23::AID**::3xFLAG animals monitoring the expression of NHR-23 3XFLAG across two time courses, 4-28 hours and 22-34 hours. Marker size (in kDa) is provided. Stain-free analysis, which visualizes total protein on the membrane, is provided as a loading control. The blots are representative of three experimental replicates. (D) Cartoons of predicted protein isoforms expressed during larval development based on Nanopore direct mRNA sequencing data (Roach et al., 2020). All of the predicted isoforms contain a Ligand Binding Domain (LBD) while only two of the three have a DNA Binding Domain (DBD). The predicted size of each isoform is listed to the right of the structure in amino acids (aa) and kDa. The AID*::3xFLAG fusion is predicted to add 9 kDa.

**Fig. 2. Distinct phenotypes are observed when NHR-23 is depleted early or late in L1 larvae.** (A) Schematic of the experimental set-up. Synchronized L1 larvae were grown on control media (light grey bands) and transferred to 4mM auxin (dark grey bands) every 2 hours. Animals remained on auxin until they were imaged at 20 hours post-release. (B) Anti-FLAG immunoblot to monitor NHR-23 depletion. Synchronized *nhr-23::AID*::3xFLAG; TIR1* and *TIR1* animals were grown on MYOB plates for 12 hours, which corresponded to the peak in L1 expression from Figure 1C. Animals were then shifted onto control or auxin plates and lysates were collected at the indicated time points. Marker size (in kDa) is provided. An anti-alpha-tubulin immunoblot is provided as a loading control. The blots are representative of three experimental replicates.
(C) Representative images of phenotypes observed when *nhr-23::AID*::3xFLAG; TIR1* animals were exposed to auxin in the first larval stage. (D) Percent of animals of the indicated genotypes with unshed cuticles and morphological abnormalities following exposure to auxin. The number of animals scored (n) is provided.

**Fig. 3. NHR-23 depletion causes developmental delay.** (A) Animals of the indicated genotype were synchronized and shifted onto auxin at 25 hours post-release and imaged 23 hours later (48 hours post-release). Animals were staged based on vulval morphology (Mok et al., 2015). L4 larval stages were grouped as Early L4 (4.0-4.2), Mid L4 (4.3-4.5), and Late L4 (4.6-4.9). (B) Representative images. The position of the vulva is highlighted with a white box. (C) *nhr-23::AID; TIR1* animals were treated as in (A) and staged after 48 and 72 hours on auxin. (D) Representative images. (E) Synchronized *nhr-23::AID; TIR1* L1 larvae were released on auxin and scored for molting defects and death 48 and 72 hours post-release. (F) Representative images. Images are representative of 100 animals examined over the course of two experiments. The number of animals assayed for each genotype and condition is indicated at the top of the graph in A, C, and E. Scale bars=20 µm. A zoomed inset is provided for the auxin-treated *nhr-23::AID, TIR1* images in B and D to highlight vulval morphology.

**Fig. 4. NHR-23 regulates oscillating genes involved in aECM biogenesis, lipid transport, and signal transduction.** (A) Radar chart plotting amplitude over the phase of peak expression of *nhr-23*-regulated genes from Kouns *et al.* (2011). The dotted circles indicated amplitude, with the innermost circle representing an amplitude of 1 and the outermost circle representing an amplitude of 4. (B) Average signal from NHR-23 ChIP-seq data (Gerstein et al., 2010) for *nhr-23*-regulated oscillating genes which peak phases between 0º-120º (Early), 120-240º (Middle), and 240º-360º. For reference, *nhr-23* mRNA peaks at 178.11º. Signal is plotted relative to transcription start site (TSS) and transcription end site (TES). The average NHR-23 signal for all 21,600 *C. elegans* genes (All genes) and the 20% of genes with the lowest expression (No expression) are shown for reference. The mean signal is plotted with a line and the mean's 95% confidence interval is indicated by the shaded area. (C) The data from (A) was plotted as a scatter plot and functionally annotated (see Table S1). To provide developmental context, we converted the 360º oscillation to developmental timing over a 9 hour larval stage, such as the L3 or L4 stage at 20ºC. In this context, 1 hour=40º and this converted developmental time is used in B and C. *nhr-23* mRNA has a peak phase of 178.11º (4.45 hours) with an

amplitude of 2.11 (Meeuse et al., 2020).The green shaded area represents NHR-23 expression based on RNA-seq (Meeuse et al., 2020), imaging (Figure 1B), and western blotting data (Figure 1C). Dotted lines indicate boundaries between the early, middle, and late *nhr-23*-regulated oscillating genes from B.

**Fig. 5. NHR-23-depletion causes reduced expression of an *nas-37p::GFP::PEST* promoter reporter.** (A) *nas-37p::GFP::PEST* expression time course. *nhr-23::AID, TIR1; nas-37p::GFP::PEST* animals were synchronized and released on control or auxin plates and scored for head or hypodermal GFP expression every two hours. Fifty animals per time point were scored in two independent experiments and the percentage of animals expressing GFP are presented. (B) Representative images of *nhr-23::AID, TIR1, nas-37p::GFP::PEST* animals grown on control or auxin plates at the indicated time points. Scale bars=20 µm.

**Fig. 6. NHR-23-depletion causes ROL-6 and NOAH-1 localization defect and reduced expression and mislocalization of BLI-1.** (A) ROL-6::mNG is first observed internally in epidermal cells 14-16 hours post-release. (B) Representative GFP images of *nhr-23::AID; TIR1, rol-6::mNeonGreen::3xFLAG* (*rol-6::mNG*) animals grown on control or auxin plates. Arrow indicates gap over seam cells (C) Representative images of *nhr-23::AID; TIR1, rol-6::mNG* animals grown on auxin with a corset phenotype. Corset is indicated by arrow. ROL-6::mNG is first observed internally in epidermal cells 14-16 hours post-release. BLI-1::mNG is first observed internally in L4.5 animals (D) where it also localized to annuli (E). Representative GFP and DIC images of *nhr-23::AID; TIR1, bli-1::mNeonGreen::3xFLAG* (*bli-1::mNG*) animals grown on control or auxin plates. Patch of BLI-1::mNG indicated by arrow. (G) Representative GFP and DIC images of the indicated tissues of *noah-1::mNeonGreen::3xFLAG* (*noah-1::mNG*), *nhr-23::AID; TIR1,* animals grown on control or auxin plates. NOAH-1::mNG gap over seam cells, and localization to excretory duct and rectum are indicated by arrows. The number of animals examined and for which the images are representative from two biological replicates is shown in A-G. Scale bars=20 µm for all images except the *noah-1::mNG* excretory duct, rectal epithelium, and vulva (scale bar=5 µm for these images).

**Fig. 7. Depletion of NHR-23 leads to a defective cuticle barrier** (A) Permeability to Hoechst 33258 dye. Synchronized animals of the indicated genotype were shifted onto control or auxin plates at 25 hours post-release and grown for 24 hours. Animals were washed off plates and incubated with the membrane impermeable Hoechst 33258 dye and scored for nuclear staining in the head and body. The data are from two biological replicates. Scale bars=20µm. Non-nuclear fluorescence in the body is background. (B) Representative images of GFP expression in animals of the indicated genotype following an early and late shift to control or auxin plates. The images are representative of 50 animals observed during each of two experimental replicates. (C) Anti-GFP immunoblot analysis of *nlp-29::*GFP expression. Marker size (in kDa) is provided. Stain-free analysis, which visualizes total protein on the membrane, is provided as a loading control. The blots are representative of two experimental replicates. (D) *nhr-23::AID; TIR1* and *TIR1* animals were added to 20µl of $dH_20$ and viability was assessed every five minutes. 10 animals were assayed for each genotype and condition with three biological replicates.

**Fig. 8. *nhr-23* is necessary in seam cells for developmental progression, molting and BLI-1 localization.** (A) Tissue-specific RNAi strains used in this experiment. A timed egg lay of animals of the indicated genotype were performed on control or *nhr-23* RNAi plates and plates were scored three days later. The number of progeny scored from two biological replicates is indicated. (B) Developmental delay was scored in the indicated strains and classified as a failure to reach adulthood after 72 hours of growth. (C) Molting defects were scored in the indicated strains and included animals trapped in cuticles, animals dragging cuticles, and animals with cuticle corsets.

**Supp Fig legends**

**Fig. S1. NHR-23::GFP expression in hypodermal tissue.** Representative image of NHR-23 expression in *nhr-23::GFP::AID*::3xFLAG; TIR-1* L4 animals. NHR-23 expression is seen in the hypodermis and developing germline, as described in Ragle et al. 2020. White arrows to seam cells expressing GFP and yellow arrows pointing to hyp cells expressing GFP.

**Fig. S2. *nhr-23* isoforms detected by Nanopore direct mRNA sequencing.** Gene model diagrams of the *nhr-23* isoforms from the "observed isoforms" track on the ENSEMBL genome track. These are isoforms confirmed by direct mRNA sequencing (Roach et al., 2020). The top tracks are of the full *nhr-23* gene, including the *nhr-23c* isoforms, which contain a large first intron. The middle tracks are a zoomed in view starting at the *nhr-23b* transcription start site. The bottom tracks are further zoomed in to depict the alternative 3' splice site usage that generates *nhr-23b* and *nhr-23f*.

**Fig. S3. Late depletion of NHR-23 in L1 leads to animals persisting in L2/L3.** Synchronized *nhr-23::AID*::3xFLAG; TIR1* and *TIR1* animals were grown on MYOB media and shifted to auxin or control plates at 16 hours post release. 30 animals for each genotype and condition were staged 48 hours post shift based on vulval morphology (Mok et al., 2015). L4 larval stages were grouped as Early L4 (4.0-4.2), Mid L4 (4.3-4.5), and Late L4 (4.6-4.9). Percentage of animals in each stage is displayed for each genotype and condition. Data are from two experimental replicates and 30 animals were scored for each strain.

**Fig. S4. NHR-23 depletion causes developmental delay which is *daf-16*-independent.** (A) Depiction of the M cell mesoblast cell divisions in L1 larvae created with BioRender.com. Newly hatched animals are born with a single M cell, which undergoes the indicated set of divisions to produce 16 descendents at the L1/L2 molt. An *hlh-8p::GFP* reporter can be used to monitor M cell divisions in living animals. (B and C) Animals of the indicated genotype were synchronized and shifted to either auxin or control plates at either 3 (early shift) or 9 hours (late shift) post-release and imaged at 24 hours post-release. Two biological replicates were performed and animals examined are provided in (C). (B) Representative images of animals of the indicated genotypes on auxin plates. (C) M cell quantification for animals of the indicated genotype shifted to control or auxin plates. Mean and standard deviation are labeled. The number of animals assayed for each genotype and condition is indicated at the top of the graph (* two-tailed T-test $p<0.0001$). (D) M cell quantitation for synchronized animals of the indicated genotype

shifted to auxin plates at 3 hours post-release and imaged 21 hours later (24 hours post-release). Mean and standard deviation labeled. The number of animals assayed for each genotype and condition is indicated at the top of the graph (* two-tailed T-test p<0.0001).

**Fig. S5. NHR-23 enrichment around genes.** Average signal over all aligned genes from two NHR-23 ChIP-seq replicates (Gerstein et al., 2010). The y-axis indicates non-normalized read coverage. The mean signal is plotted with a line and the mean's 95% confidence interval is indicated by the shaded area. TSS=transcription start site; TES=transcription end site.

**Fig. S6. Validation of *bli-1, noah-1,* and *rol-6* mNeonGreen::3xFLAG knock-in strains.** (A) Brood size analysis of animals of the indicated genotype. Anti-FLAG immunoblots on lysates from *rol-6::mNG* and *noah-1::mNG* mid-L4 animals (B) and *bli-1::mNG* adult animals (C). An age matched WT control is included in each experiment. Marker size (in kDa) is provided and an anti-alpha-tubulin immunoblot was used as a loading control. The mNeonGreen::3xFLAG tag adds ~33.2 kDa and the predicted sizes are: ROL-6::mNG=67.9 kDa; NOAH-1::mNG=148.9 kDA; BLI-1::mNG=138.5 kDa.

**Fig. S7. Expression patterns of *SCMp* and *wrt-2* promoter reporters.** *SCMp::NLS::mScarlet* promoter reporters express robustly in the seam cells (A) with weak expression in the hypodermis (B) in a subset of animals. *wrt-2p::NLS::mScarlet* is expressed in the hypodermis and seam cells (C and D). In some animals seam cell expression is lacking. In C, arrows point to two seam cells, one with reporter expression and one lacking it. Two biological replicates were performed and the number of animals for which each image is representative is indicated.

**Fig. S8. JDW525 animals are permissive for RNAi knockdown in seam, hypodermal, and intestinal cells.** JDW 525 [*his-72(wrd142[mNeonGreen::his-72]) III ; jsTi1493 {mosL loxP [wrdSi65(SCMp::rde-1 CDS+3'UTR)] FRT3::mosR} IV ; rde-1 (ne300) V]* animals grown on control RNAi display HIS-72::mNG expression in hypodermal, intestinal, germline, vulval, and seam cells. mNeonGreen RNAi caused reduction of HIS-72::mNG

expression in seam, intestinal, and syncytial hypodermal (hyp7) cells. Vulval, germline, and head hypodermal expression was unaffected. Scale bars=20µm. Data are representative of forty animals examined over two biological replicates

## MATERIALS AND METHODS

### *C. elegans* Strains and Culture

*C. elegans* strains were cultured as originally described (Brenner, 1974), except worms were grown on MYOB instead of NGM. MYOB was made as previously described (Church et al., 1995). Animals were cultured at 20ºC for all assays, unless otherwise indicated. For general strain propagation, animals were grown at 15ºC according to standard protocols. Brood sizes were performed picking L4 larvae to individual wells of a 6-well plate seeded with OP50 and incubating the plate at 20ºC. Animals were transferred to new plates daily over 4 days. Two days post-transfer, the number of hatched progeny and unfertilized eggs were scored.

**Strains used in this study:**

| Strain | Construction | Genotype |
|---|---|---|
| JDW180 | Microinjection | *wrdEx12[SCMp::NLS-mScarlet (dpi)-tbb-2 3'UTR + pCFJ90 (myo-2p::mCherry)]* |
| JDW258 | Ashley *et al.,* 2021 | *wrdSi22 [eft-3p::TIR1::F2A::mTagBFP2::AID*::NLS::tbb-2 3'UTR+SEC, I:-5.32] ; nhr-23(kry61(nhr-23::AID*-TEV-3xFLAG)) I* |
| JDW259 | Ashley *et al.,* 2021 | *wrdSi55[eft-3p::TIR1::F2A::mTagBFP2::AID*::NLS::tbb-2 3'UTR, I:-5.32] ; nhr-23(kry61(nhr-23::AID*-TEV-3xFLAG)) I* |
| JDW322 | Microinjection | *wrdEx29[wrt-2p::NLS-mScarlet (dpi)-tbb-2 3'UTR]* |
| JDW348 | Crossing | *ieSi57 [Peft-3::TIR1::mRuby::unc-54 3'UTR, cb-unc-119(+?)] II; frIs7 [nlp-29p::GFP + col-12p::DsRed] IV* |

| | | |
|---|---|---|
| JDW349 | Crossing | *nhr-23(kry61(nhr-23::AID*-TEV-3xFLAG))I; ieSi57 [Peft-3::TIR1::mRuby::unc-54 3'UTR, cb-unc-119(+?)] II; frIs7 [nlp-29p::GFP + col-12p::DsRed] IV.x* |
| JDW330 | Crossing | *rde-1 (ne300) V.; jsTi1493 [mosL loxP mex-5p FLP sl2 mNeonGreen rpl-28p FRT GFP-HIS-58 FRT3 mosR] IV* |
| JDW354 | Crossing | *wrdSi60[eft-3p::TIR1::F2A::mTagBFP2::AID*::NLS::tbb-2:tbb-2 3'UTR, I:-5.32] I; ayIs6 [hlh-8::GFP fusion + dpy-20(+)] X* |
| JDW355 | Crossing | *wrdSi61[eft-3p::TIR1::F2A::mTagBFP2::AID*::NLS::tbb-2:tbb-2 3'UTR, I:-5.32] ; nhr-23(kry61(nhr-23::AID*-TEV-3xFLAG)) I; ayIs6 [hlh-8::GFP fusion + dpy-20(+)] X* |
| JDW356 | Crossing | *wrdSi59[eft-3p::TIR1::F2A::mTagBFP2::AID*::NLS::tbb-2 3'UTR, I:-5.32], daf-16(mu86) I; ayIs6 [hlh-8::GFP fusion + dpy-20(+)] X* |
| JDW357 | Crossing | *wrdSi59[eft-3p::TIR1::F2A::mTagBFP2::AID*::NLS::tbb-2 3'UTR, I:-5.32], nhr-23(kry61(nhr-23::AID*-TEV-3xFLAG)), daf-16(mu86) I; ayIs6 [hlh-8::GFP fusion + dpy-20(+)] X* |
| JDW370 | Microinjection | *jsTi1493 {mosL::loxP::mex-5p::FLP::sl2::mNeonGreen::rpl-28p::FRT [wrdSi64**(SEC::loxP::SCMp::rde-1 CDS+3'UTR)**] FRT3::mosR} IV ; rde-1 (ne300) V* |
| JDW371 | SEC excision of JDW370 | *jsTi1493 {mosL loxP [wrdSi65(SCM**p::rde-1 CDS+3'UTR**)] FRT3::mosR} IV ; rde-1 (ne300) V* |
| JDW395 | Crossing | *wrdSi73[eft-3p::TIR1::F2A::mTagBFP2::AID*::NLS::tbb-2 3'UTR] ; nhr-23(kry61(nhr-23::AID*-TEV-3xFLAG)) I; oxIs134[Pnas-37::GFP:rODC(pest)(pWD95@90ng/ul),lin-15(+)]* |
| JDW459 | Microinjection | *nhr-23(kry61(nhr-23::AID*-TEV-3xFLAG))I; ieSi57 [Peft-3::TIR1::mRuby::unc-54 3'UTR, cb-unc-119(+?)] II* |
| JDW463 | Microinjection | *nhr-23(kry61(nhr-23::AID*-TEV-3xFLAG)) I ; ieSi57 [Peft-3::TIR1::mRuby::unc-54 3'UTR, cb-unc-119(+?)] , bli-1(wrd122[bli-1::internal mNeonGreen (dpi)::3xFLAG::linker]) II* |
| JDW472 | Microinjection | *rol-6(wrd123[rol-6::C-term mNeonGreen (dpi)::3xFLAG::linker]) I ; jsTi1493 wrdSi65[SCMmin::pes-10delta::rde-1 CDS+3'UTR in pLF3FShC]IV; rde-1(ne300) V.* |

| | | |
|---|---|---|
| JDW475 | Microinjection | *noah-1(wrd126[noah-1::internal mNeonGreen (dpi)::3xFLAG::linker]) , nhr-23(kry61(nhr-23::AID*-TEV-3xFLAG)) I ; ieSi57 [Peft-3::TIR1::mRuby::unc-54 3'UTR, cb-unc-119(+?)] II* |
| JDW509 | Microinjection | *jsTi1493 {mosL::loxP::mex-5p::FLP::sl2::mNeonGreen::rpl-28p::FRT [wrdSi96**(SEC::loxP::semo-1 (Y37A1B.5)p::rde-1 CDS+3'UTR)**] FRT3::mosR} IV ; rde-1 (ne300) V* |
| JDW510 | SEC excision of JDW509 | *jsTi1493 {mosL loxP [wrdSi97(**semo-1p::rde-1 CDS+3'UTR**)] FRT3::mosR} IV ; rde-1 (ne300) V* |
| JDW525 | Microinjection | *his-72(wrd142[mNeonGreen::his-72]) III ; jsTi1493 {mosL loxP [wrdSi65(SCMp::rde-1 CDS+3'UTR)] FRT3::mosR} IV ; rde-1 (ne300) V* |
| KRY87 | (Zhang et al., 2015) | *nhr-23(kry61(nhr-23::AID*-TEV-3xFLAG))I* |
| KRY88 | Zhang et al., 2015 | *nhr-23(kry61(nhr-23::AID*-TEV-3xFLAG))I; ieSi57 [Peft-3::TIR1::mRuby::unc-54 3'UTR, cb-unc-119(+?)] II* |
| NM5179 | Nonet, 2020 | *jsTi1493 [mosL loxP mex-5p FLP sl2 mNeonGreen rpl-28p FRT GFP-HIS-58 FRT3 mosR] IV* |

Strains provided by the *Caenorhabditis* Genetics Center:

| **Strain** | **Genotype** |
|---|---|
| N2 | Wild-type |
| CA1200 | *ieSi57 [Peft-3::TIR1::mRuby::unc-54 3'UTR, cb-unc-119 (+?)] II* (Zhang *et al.,* 2015) |
| CF1038 | *daf-16(mu86) I* *(Lin et al., 1997)* |
| PD4666 | *ayIs6 [hlh-8::GFP fusion + dpy-20(+)] X (Harfe et al., 1998)* |

| | |
|---|---|
| QK52 | *rde-1(ne219) V ;*<br>*xkIs99(wrt-2p::rde-1::unc-54 3'UTR) (Melo and Ruvkun, 2012)* |
| VP303 | *rde-1(ne219) V ;*<br>*kbIs7[nhx-2p::rde-1 + rol-6(su1006)]) (Espelt et al., 2005)* |
| JU2039 | *mfIs70*<br>*[lin-31p::rde-1 + myo2p::GFP] IV ; rde-1(ne219) V (Barkoulas et al., 2013)* |
| WM118 | *rde-1(ne300) V ; neIs9(neIs9 [myo-3::HA::RDE-1 + rol-6(su1006)]) X* (Watts et al., 2020) |
| MGH171 | *alxIs9 [vha-6p::sid-1::SL2::GFP] sid-1(qt9) V (Melo and Ruvkun, 2012)* |
| NM5179 | *jsTi1493 [mosL loxP mex-5p FLP sl2 mNeonGreen rpl-28p FRT GFP-HIS-58 FRT3 mosR] IV (Nonet, 2020)* |
| WM45 | *rde-1(ne300) V* (Tabara et al., 1999) |
| IG274 | *frIs7 [nlp-29p::GFP + col-12p::DsRed] IV* (Pujol et al., 2008) |

**Other strains**

EG3200 *oxIs134[Pnas-37::GFP:rODC (pest) (pWD95@90ng/ul),lin-15(+)]; lin-15(n765ts)* X (Davis et al., 2004) was provided by D. Fay (U Wyoming).

**Genome editing and transgenesis**

mNeonGreen::3xFLAG knock-ins into *bli-1, noah-1,* and *rol-6* and *mNeonGreen* knock-ins into *his-72* were generated by injection of Cas9 ribonucleoprotein complexes [700 ng/ul IDT Cas9, 115 ng/ul crRNA and 250 ng/ul IDT tracrRNA] and a dsDNA repair template (25-50 ng/ul) created by PCR amplification of a plasmid template (Paix et al., 2014; Paix et al., 2015). The PCR products were melted to boost editing efficiency, as previously described (Ghanta and Mello, 2020). crRNAs used are provided in Table S5. Oligonucleotides used for repair template generation from template pJW2172 (Ashley et al., 2021) and for genotyping are provided in Table S6. Genomic and knock-in sequences are provided in File S1. Plasmids used are provided in Table S7. To generate JDW371 and JDW510 (seam cell and hypodermal-specific tissue-specific RNAi) we crossed a

*jsTi1493* landing pad for recombination-mediated cassette exchange (RMCE)(Nonet, 2020) into an *rde-1(ne300)* null mutant, generating JDW330. We used GIbson cloning to introduce a promoterless *rde-1* genomic coding sequence+3'UTR fragment into the RMCE integration vector pLF3FShC (Nonet, 2020), creating pJW2247. This vector can be linearized with *Avr*II+*Bsi*WI double-digestion and promoters can be introduced by Gibson cloning (Gibson et al., 2009). We generated a *SCMp* (seam cell-specific) and *semo-1p* (hypodermis specific) by Gibson cloning promoters into linearized pJW2247, constructing pJW2236 and pJW2264, respectively. These vectors were integrated into *jsTi1493* landing pad in JDW330 using RMCE, as described (Nonet, 2020). *wrt-2p* and *SCMp* promoter reporters were constructed in pJW1836 (*NLS::mScarlet::tbb-2 3' UTR*)(Ashley et al., 2021) by Gibson cloning. Plasmids were injected into N2 animals at 50 ng/µl with a pCFJ90 co-injection marker at 10 ng/µl for the *SCMp* promoter reporter and a pRF4 co-injection marker at 50 ng/µl for the *wrt-2* promoter reporter (Frøkjaer-Jensen et al., 2008; Mello et al., 1991). Transgenic lines propagating extrachromosomal arrays were generated as previously described (Mello et al., 1991). Sequence files for plasmids are provided in File S2. Primers and cloning details are available upon request.

**Auxin treatment**

Control and auxin media/plates were made as described in Ragle et al. 2020. Control media consisted of MYOB agar+0.25% ethanol. Auxin media was made by dissolving indole 3-acetic acid (IAA; Alfa Aesar, AAA1055622) in 100% ethanol to 1.6 M and then mixing it into melted MYOB agar at 55°C to a final concentration of 4 mM prior to pouring plates. Control plates contained 0.25 % ethanol. Temperature of the media was monitored with a Lasergrip 1080 infrared thermometer gun (Etekcity). Plates were seeded with *E. coli* OP50 and incubated overnight at room temperature. Plates were stored for up to one month at 4ºC prior to use. For most auxin treatment experiments, animals were synchronized by alkaline bleaching (dx.doi.org/10.17504/protocols.io.j8nlkkyxdl5r/v1). The collected eggs were incubated in M9 buffer supplemented with 5 mg/mL cholesterol at 20ºC for 24 hours and arrested L1 larvae were released onto the indicated type of MYOB plate. For the experiment in Table S1 a timed egg lay was performed. Twenty adult hermaphrodites animals of the indicated genotype were picked onto control (0.25%

ethanol) or auxin (4 mM IAA) plates and allowed to lay eggs for 2 hours. The adult animals were removed and plates were incubated for 48 hours at 25ºC.

**Microscopy**

Synchronized animals were collected from MYOB, control, or auxin plates by either picking or washing off plates. For washing, 1000 µl of M9 + 0.05% gelatin was added to the plate or well, agitated to suspend animals in M9+gelatin, and then transferred to a 1.5 ml tube. Animals were spun at 700xg for 1 min. The media was then aspirated off and animals were resuspended in 500µl M9 + 0.05% gelatin with 5 mM levamisole. 12 µl of animals in M9 + 0.05% with levamisole solution were placed on slides with a 2% agarose pad and secured with a coverslip. For picking, animals were transferred to a 10 µl drop of M9+5 mM levamisole on a 2% agarose pad on a slide and secured with a coverslip. Images were acquired using a Plan-Apochromat 40x/1.3 Oil DIC lens or a Plan-Apochromat 63x/1.4 Oil DIC lens on an AxioImager M2 microscope (Carl Zeiss Microscopy, LLC) equipped with a Colibri 7 LED light source and an Axiocam 506 mono camera. Acquired images were processed through Fiji software (version: 2.0.0- rc-69/1.52p). For direct comparisons within a figure, we set the exposure conditions to avoid pixel saturation of the brightest sample and kept equivalent exposure for imaging of the other samples.

**Phenotypic analysis**

For the phenotypic analysis in Figure 2, synchronized CA1200 or KRY88 larvae were released onto MYOB plates and then shifted onto control or auxin plates every two hours up to 16 hours. Animals were collected as described in the Microscopy section and imaged by DIC microscopy to score for morphology and shedding of the L1 cuticles. For the M cell lineage experiments in Figures S5, synchronized animals of the indicated genotypes were released onto MYOB plates and shifted onto control or auxin plates at 3 hours (early shift) or 9 hours (late shift) post-release and then imaged at 24 hours post-release, as described in the Microscopy section. M cells were counted and recorded. For the L3 shift experiments (Fig. 3A-D) synchronized animals of the indicated genotype were grown on MYOB. At 25 hours post-release, they were shifted onto 6-well control or auxin

MYOB plates seeded with OP50. 24, 48, or 72 hours later animals were collected as described in the Microscopy section and imaged by DIC microscopy using a 63x lens to stage animals according to vulval morphology (Mok et al., 2015). For the analyses in Figure 3E-F, synchronized *nhr-23::AID, TIR1* larvae were released on auxin plates and scored for viability and molting defects 48 and 72 hours later. For the reporter timecourse, synchronized *nhr-23::AID, TIR1, nas-37p::GFP::PEST* animals were released on control or auxin plates. They were then scored for GFP expression using a PlanApo 5.0x/0.5 objective on a M165 FC stereomicroscope (Leica) equipped with an X-cite FIRE LED lightsource (Excelitas) and long pass GFP filter set (Leica #10447407). We scored GFP expression in the head and hypodermis and did not score rectal GFP expression, as expression perdured in this tissue after head and hypodermal GFP expression ceased.

**Barrier assays**

Hoechst 33258 staining was performed as described previously (Moribe et al., 2004), except that we used 10 µg/ml of Hoechst 33258 as in Ward et al. (2014). Two biological replicates were performed examining 50 animals per experiment. The number of animals with either head or hypodermal nuclei staining with Hoechst 33258 were scored under a 10x DIC objective. Representative images were then taken with equivalent exposures using a 63x Oil DIC lens, as described in the imaging section. Hypo-osmotic stress sensitivity assays were performed on L4 stage larvae as described (Ward et al., 2014), except we used 20µl of $dH_20$. Each strain was assayed in triplicate.

**Western Blots**

Animals were synchronized by alkaline bleaching, as described in the “Auxin Treatment” section. For the blot in Fig. S6B, 30 animals of the indicated genotype and stage were picked into 30 µl of M9+0.05% gelatin and 10 µl of 4x Laemmli sample buffer was added and then samples were heated at 95ºC for 5 minutes and stored at -80ºC until they were resolved by SDS-PAGE (described in following paragraph). For the blot in Fig. S6B, ~1000 animals of the indicated genotype were washed out of a 6 cm MYOB plate, transferred to a 1.5 ml tube and washed twice more with M9+0.05% gelatin, as previously described (Vo et al., 2021). Animals were pelleted and flash frozen in 50 µl of M9+gelatin

in liquid nitrogen. Samples were stored at -80ºC. Lysates were made by adding 50 µl of 2xRIPA buffer (Sigma SIAL-20-188) supplemented with 2 mM PMSF and Protease Inhibitor Cocktail Set III, EDTA-Free (Calbiochem #539134) and sonicating in a Diagenode Bioruptor for 30 cycles of 30 seconds on/30 seconds off. Laemmli sample buffer was added to 1X and samples were heated at 70ºX for 10 minutes to denature the protein. For the remaining blots, animals of the indicated genotype were washed out of wells on a 6-well plate at the indicated timepoints with M9+0.05% gelatin (VWR, 97062-620), transferred to a 1.5 ml tube and washed twice more with M9+0.05% gelatin, as previously described (Vo et al., 2021). Animals were pelleted, transferred in a 100 µl volume to a new 1.5 ml tube, and flash frozen in liquid nitrogen, then stored at -80ºC. Prior to SDS-PAGE, samples were freeze-cracked twice in liquid nitrogen or on dry ice, Laemmli sample buffer was added to 1X and samples were heated to 95ºC for 5 minutes. For the western blots in Figure 1C 6000 KRY88 animals per well were transferred onto a 6-well MYOB plate seeded with OP50. For the western blot in Figure 2B, 6000 synchronized KRY88 animals were plated onto control or auxin plates. Control animals were harvested at peak NHR-23 expression (12 hours of growth on control plates) and auxin-treated animals were shifted onto auxin at this time and samples were taken at the indicated time points, as described above. For the western blots in Figure 7C, 500 animals of the indicated genotype were transferred into wells of a 6-well control or auxin plate seeded with OP50. Animals were incubated for 24 hours at 20ºC and collected as described above.

For the blots in Figs. 1C, 10 µl of lysate and 7.5 µl 1:1 mix of Amersham ECL Rainbow Molecular Weight Markers (95040-114) and Precision Plus Protein Unstained Standards (#1610363) was resolved by SDS-PAGE using precast 4-20% MiniProtean TGX Stain Free Gels (Bio-Rad). The blot in Fig. 7C, the lysates had more variable levels of total protein, particularly the NHR-23 depleted samples that produced an early larval arrest. Therefore we quantified the signal of the most intense band by Stain Free imaging (Posch et al., 2013) using a Bio-Rad ChemiDoc imaging system, and ran a new gel with normalized loading. The lysates in Fig. 2B, 7C, S6B and C were resolved as described adobe except we used a Spectra™ Multicolor Broad Range Protein Ladder (Thermo; #

26623). Proteins were transferred to a polyvinylidene difluoride membrane by semi-dry transfer with a TransBlot Turbo (Bio-Rad). In Figs 1C and 7C, total protein, pre- and post-transfer, was monitored using the stain-free fluorophore as described (Posch et al., 2013; Ward, 2015a). Membranes were washed in TBST and blocked in TBST+5% milk (TBST-M; Nestle Carnation Instant Nonfat Dry Milk, 25.6-Ounce, Amazon) for one hour at room temperature. Blots were rocked in primary antibodies in TBST-M overnight at 4ºC and then washed 4x5min with TBST. For primary antibodies conjugated with horseradish peroxidase (HRP) the blots were developed after the last TBST wash. Otherwise, blots were incubated with HRP-conjugated secondary antibodies in TBST-M for one hour at room temperature followed by 4x5min TBST washes and then developed as described below.

The primary antibody used for Figures 1C, 2B, and S6B and C was horseradish peroxidase (HRP) conjugated anti-FLAG M2 (Sigma-Aldrich, A8592-5x1MG, Lot #SLCB9703) at a 1:2000 dilution. Precision Protein StrepTactin-HRP Conjugate (Bio-Rad, #1610381, Lot #64426657) was included with the primary antibody at a 1:10,000 dilution to visualize the protein size standard during blot imaging for Figs 1C. For the blot in Fig. 2B, 7C, 6B and C, we used mouse anti-alpha-Tubulin 12G10 (Developmental Studies Hybridoma Bank, the "-c" concentrated supernatant at 1:2000 (Fig 7C, 2B) or 1:4000 (Fig. S6B,C). The secondary antibodies were Digital anti-mouse (Kindle Biosciences LLC, R1005) diluted 1:10,000 (Fig. 2B, 7C) or 1:20,000 (Fig. S6B,C). Blots were incubated for 5 minutes with 1 ml of Supersignal West Femto Maximum Sensitivity Substrate (Thermo Fisher Scientific, 34095) and imaged using the 'chemi high-resolution' setting on a Bio-Rad ChemiDoc MP System.

**Bioinformatics**

Figure 4A was generated in R (R Core Team). Phase and amplitude in Table S1 were converted to x and y coordinates for each gene by calculating x = amplitude * cos(phase) and y = amplitude * sin(phase). For Figure 6B and S6, L3 NHR-23 ChIP-Seq data was downloaded from http://www.modencode.org, accession ID modEncode_3837. Wig files were converted to bigwig format and loaded into the Bioconductor package SeqPlots

(cite_SeqPlots)(Huber et al., 2015; Stempor and Ahringer, 2016). A bed file with the start and end coordinates of all genes' CDS was generated and loaded into SeqPlots. SeqPlots aligned all genes by the start and end position and scaled the coding sequence of each gene to 2 kb. The average signal over all aligned genes was calculated in 25 bp windows from 1 kb upstream of the start site to 1kb downstream of the end site. For Fig. 6C the phase for the oscillating genes in Table S1 was converted to time during the molting cycle by assuming a 9 hour larval stage which make each hour=40º. The phase in hours was then plotted along the x axis and the oscillating genes' amplitude was plotted on the y axis. The gene annotation was based on the Concise Description and Automated Description downloaded from Wormbase.

**RNAi**

RNAi feeding plates were made by melting a solidified bottle of MYOB and adding Carbenicillin (25 ug/ml) and IPTG (8mM) once cooled to 55℃. dsRNA-expressing *E. coli* bacteria were streaked on LB plates with Ampicillin (100 ug/ml) and grown overnight at 37℃. A single colony was picked into 25 ml LB with 100 ug/ml Ampicillin and 12.5 ug/ml Tetracycline and shaken overnight at 37℃ at 220 RPMs. The next day, the liquid culture was pelleted and resuspended in 1.25 ml LB with 100 ug/ml Ampicillin resulting in a 20x concentration from the original overnight liquid culture. 90 ul of the liquid culture was spread per small RNAi plate and allowed to dry. The plates were incubated at room temperature in the dark for 3 days. 10 adult worms from each strain were allowed to lay eggs on plates spread with *E. coli* bacteria containing either the control plasmid L4440 or the *nhr-23* RNAi knockdown plasmid for 1-2 hours. The adults were removed and the eggs allowed to develop at 20℃ for 2 or 3 days depending on the experiment.

**Statistical Analysis**

Statistical tests and numbers of animals analyzed are detailed in figure legends.

**Competing interests**

The authors declare no competing or financial interests.

**Acknowledgements**

We thank Chris Hammell, David Matus, and Julian Ceron Madrigal for their critical reading of the manuscript. We thank David Fay, Miles Pufall, Helge Grosshans, and Ali Shariati for helpful discussions. We thank Andrew Chisholm and Jennifer Adams for providing information about *rol-6* and *bli-1* mNeonGreen knock-ins that they generated.

**Funding**

This work was funded by the National Institutes of Health (NIH) National Institute of General Medical Sciences (NIGMS) [R01 GM138701] to J.D.W. Some strains were provided by the Caenorhabditis Genetics Center, which is funded by the NIH Office of Research Infrastructure Programs [P40 OD010440]. L.C.J. was funded by an NIGMS training grant [T32 GM133391]. The anti-alpha tubulin 12G10 monoclonal antibody developed by J. Frankel and E.M. Nelson of the University of Iowa was obtained from the Developmental Studies Hybridoma Bank, created by the NICHD of the NIH and maintained at The University of Iowa, Department of Biology, Iowa City, IA 52242.

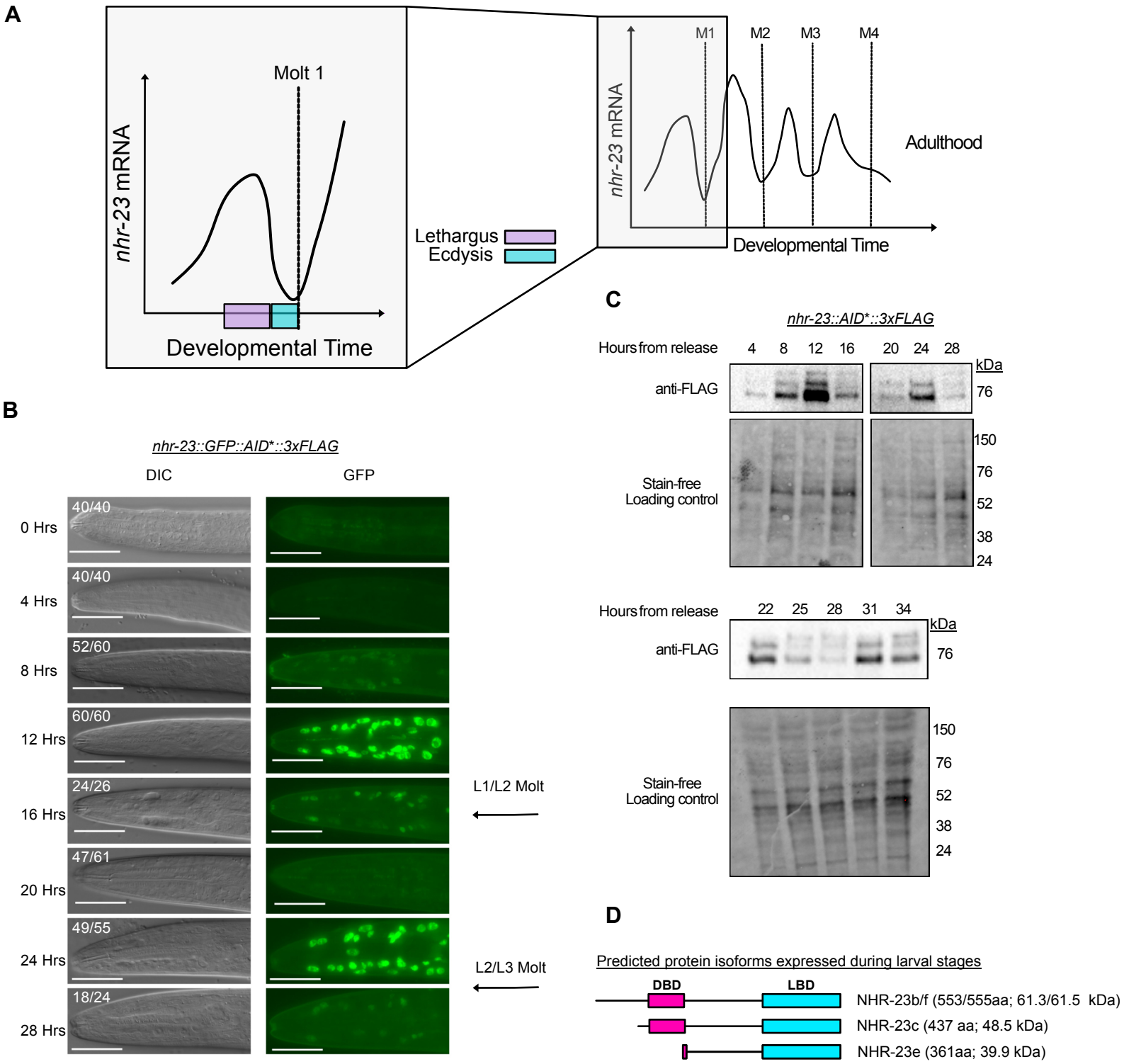
A
Molt 1
nhr-23 mRNA
Developmental Time
Lethargus
Ecdysis
M1
M2
M3
M4
nhr-23 mRNA
Adulthood
Developmental Time
B
nhr-23::GFP::AID*::3xFLAG
DIC
GFP
0 Hrs
40/40
4 Hrs
40/40
8 Hrs
52/60
12 Hrs
60/60
16 Hrs
24/26
20 Hrs
47/61
24 Hrs
49/55
28 Hrs
18/24
L1/L2 Molt
L2/L3 Molt
C
nhr-23::AID*::3xFLAG
Hours from release
4 8 12 16 20 24 28
kDa
anti-FLAG
76
Stain-free
Loading control
150
76
52
38
24
Hours from release
22 25 28 31 34
kDa
anti-FLAG
76
Stain-free
Loading control
150
76
52
38
24
D
Predicted protein isoforms expressed during larval stages
DBD
LBD
NHR-23b/f (553/555aa; 61.3/61.5 kDa)
NHR-23c (437 aa; 48.5 kDa)
NHR-23e (361aa; 39.9 kDa)

**Figure 1**

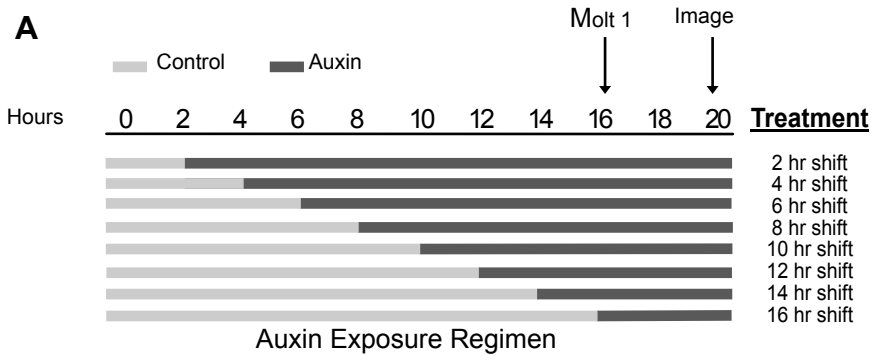


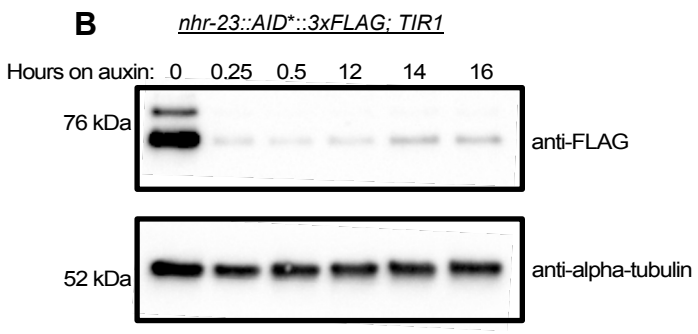


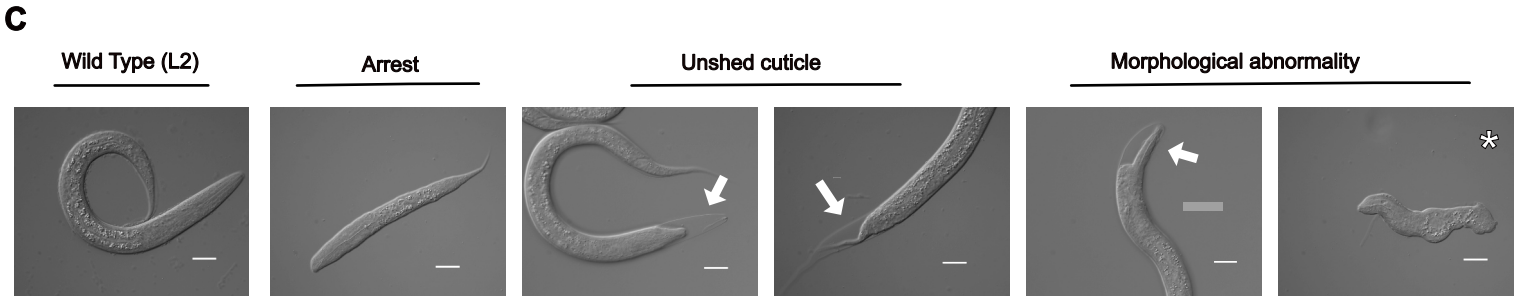


**D**

Phenotypic data for *nhr-23::AID*; *TIR1*

| Shift Hour | (n) | | % Unshed cuticle | | % Morphological abnormality | |
|---|---|---|---|---|---|---|
| | *nhr-23::AID; TIR1* | *TIR1* | *nhr-23::AID; TIR1* | *TIR1* | *nhr-23::AID; TIR1* | *TIR1* |
| *2* | *40* | *40* | 0 | *0* | 5 | *0* |
| *4* | *40* | *40* | 28 | *0* | 5 | *0* |
| *6* | *40* | *31* | 40 | *0* | 18 | *0* |
| *8* | *40* | *35* | 40 | *0* | 30 | *0* |
| *10* | *31* | *37* | 58 | *0* | 42 | *0* |
| *12* | *40* | *20* | 40 | *0* | 55 | *0* |
| *14* | *39* | *32* | 5 | *0* | 0 | *0* |
| *16* | *40* | *36* | 5 | *0* | 5 | *0* |

**Figure 2**

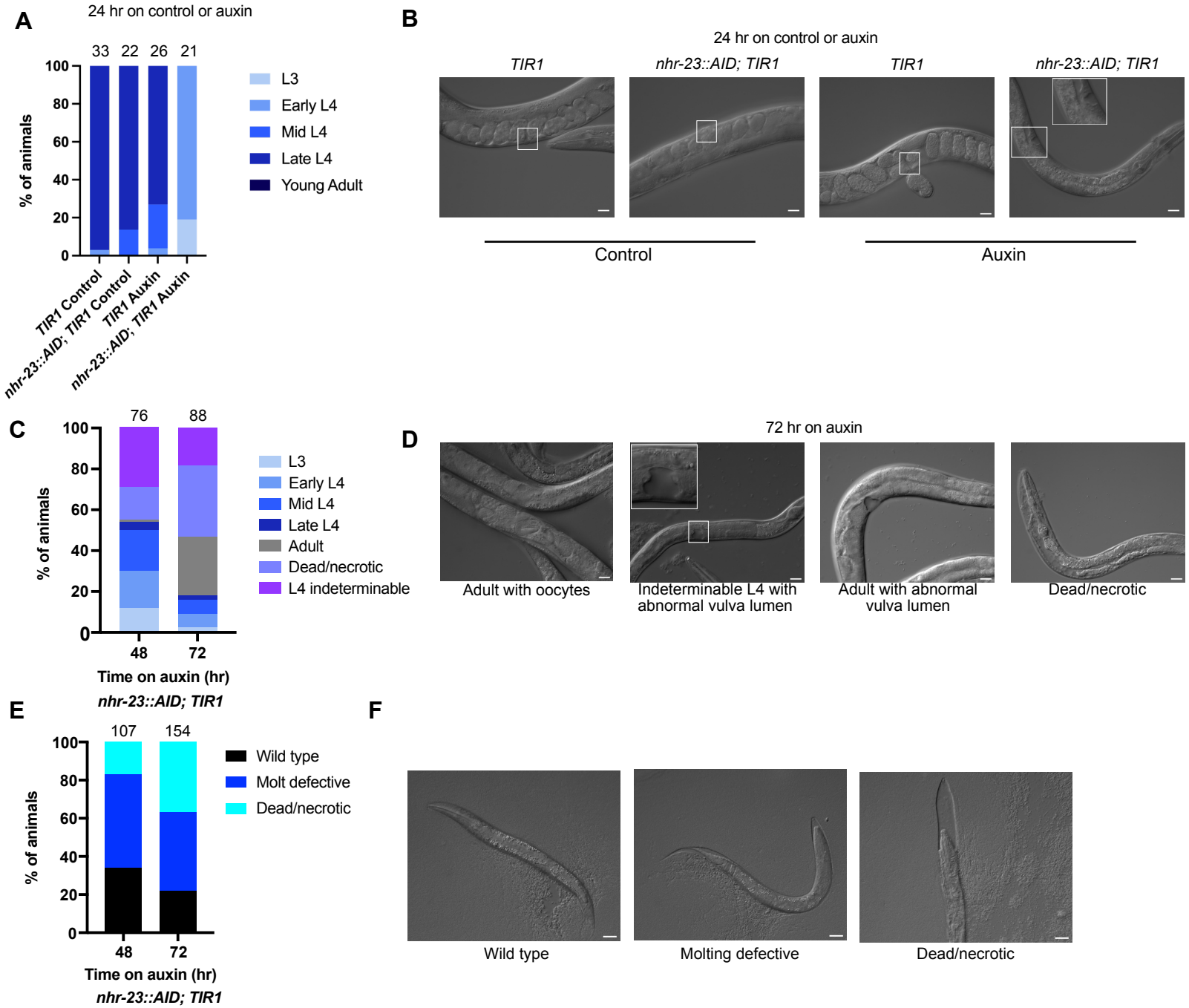
A
24 hr on control or auxin
33 22 26 21
% of animals
100
80
60
40
20
0
TIR1 Control
nhr-23::AID; TIR1 Control
TIR1 Auxin
nhr-23::AID; TIR1 Auxin
L3
Early L4
Mid L4
Late L4
Young Adult
B
24 hr on control or auxin
TIR1
nhr-23::AID; TIR1
TIR1
nhr-23::AID; TIR1
Control
Auxin
C
76 88
% of animals
100
80
60
40
20
0
48
72
Time on auxin (hr)
nhr-23::AID; TIR1
L3
Early L4
Mid L4
Late L4
Adult
Dead/necrotic
L4 indeterminable
D
72 hr on auxin
Adult with oocytes
Indeterminable L4 with abnormal vulva lumen
Adult with abnormal vulva lumen
Dead/necrotic
E
107 154
% of animals
100
80
60
40
20
0
48
72
Time on auxin (hr)
nhr-23::AID; TIR1
Wild type
Molt defective
Dead/necrotic
F
Wild type
Molting defective
Dead/necrotic

**Figure 3**

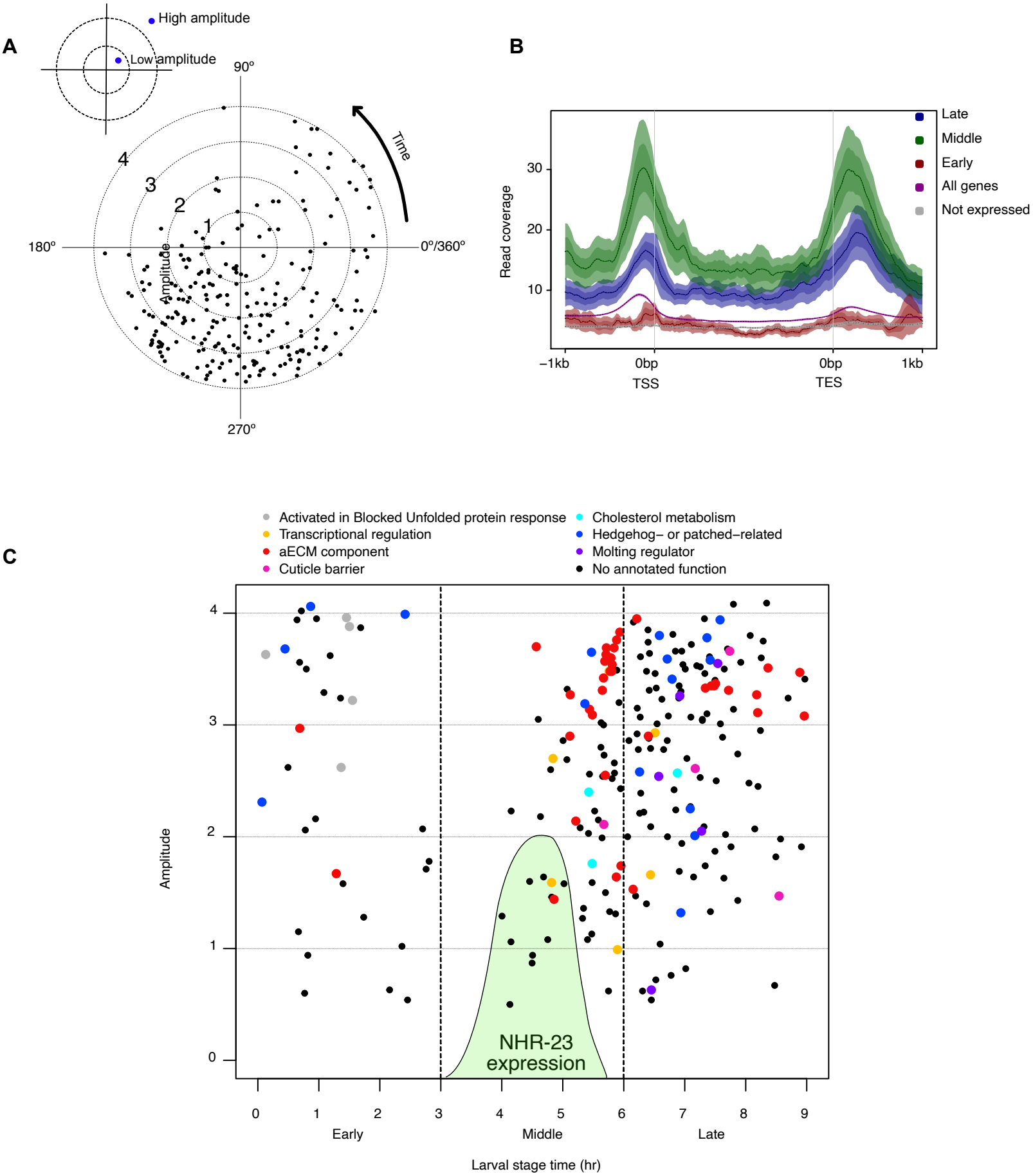
A
High amplitude
Low amplitude
90°
Time
4
3
2
1
180°
0°/360°
Amplitude
270°
B
Late
Middle
Early
All genes
Not expressed
Read coverage
30
20
10
−1kb
0bp
TSS
0bp
TES
1kb
C
Activated in Blocked Unfolded protein response
Transcriptional regulation
aECM component
Cuticle barrier
Cholesterol metabolism
Hedgehog− or patched−related
Molting regulator
No annotated function
Amplitude
NHR-23
expression
Early
Middle
Late
Larval stage time (hr)

**Figure 4**

**A**

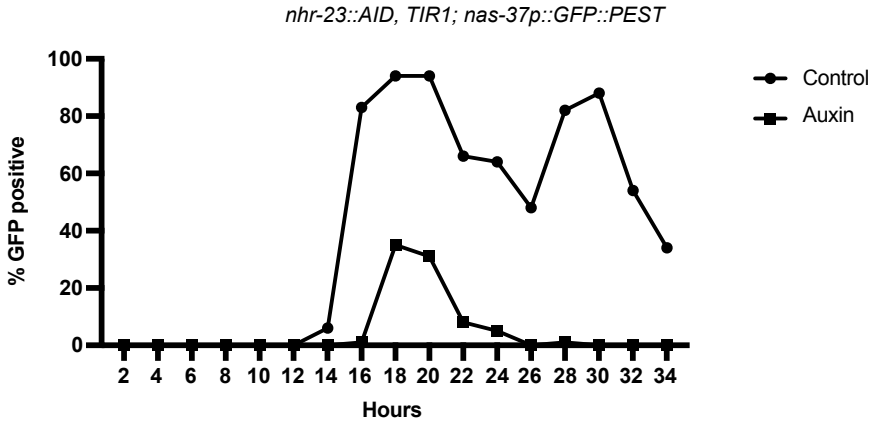
nhr-23::AID, TIR1; nas-37p::GFP::PEST
% GFP positive
100
80
60
40
20
0
2 4 6 8 10 12 14 16 18 20 22 24 26 28 30 32 34
Hours
Control
Auxin

**B**

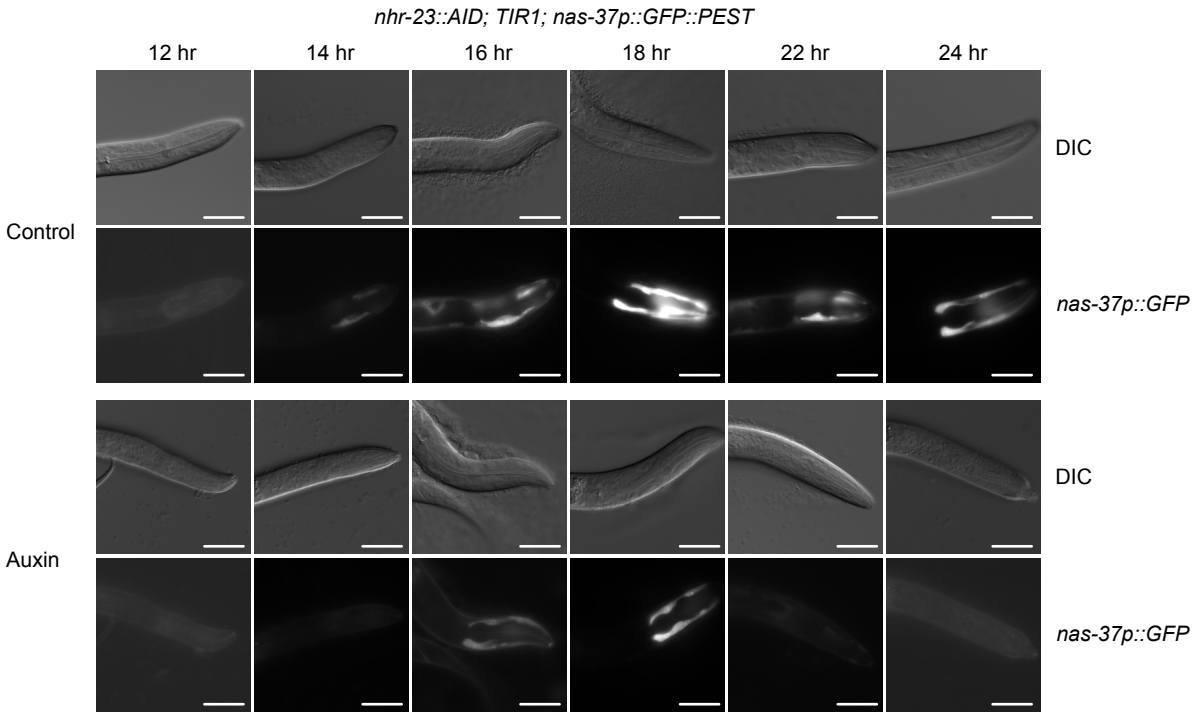
nhr-23::AID; TIR1; nas-37p::GFP::PEST
12 hr
14 hr
16 hr
18 hr
22 hr
24 hr
Control
Auxin
DIC
nas-37p::GFP
DIC
nas-37p::GFP

**Figure 5**

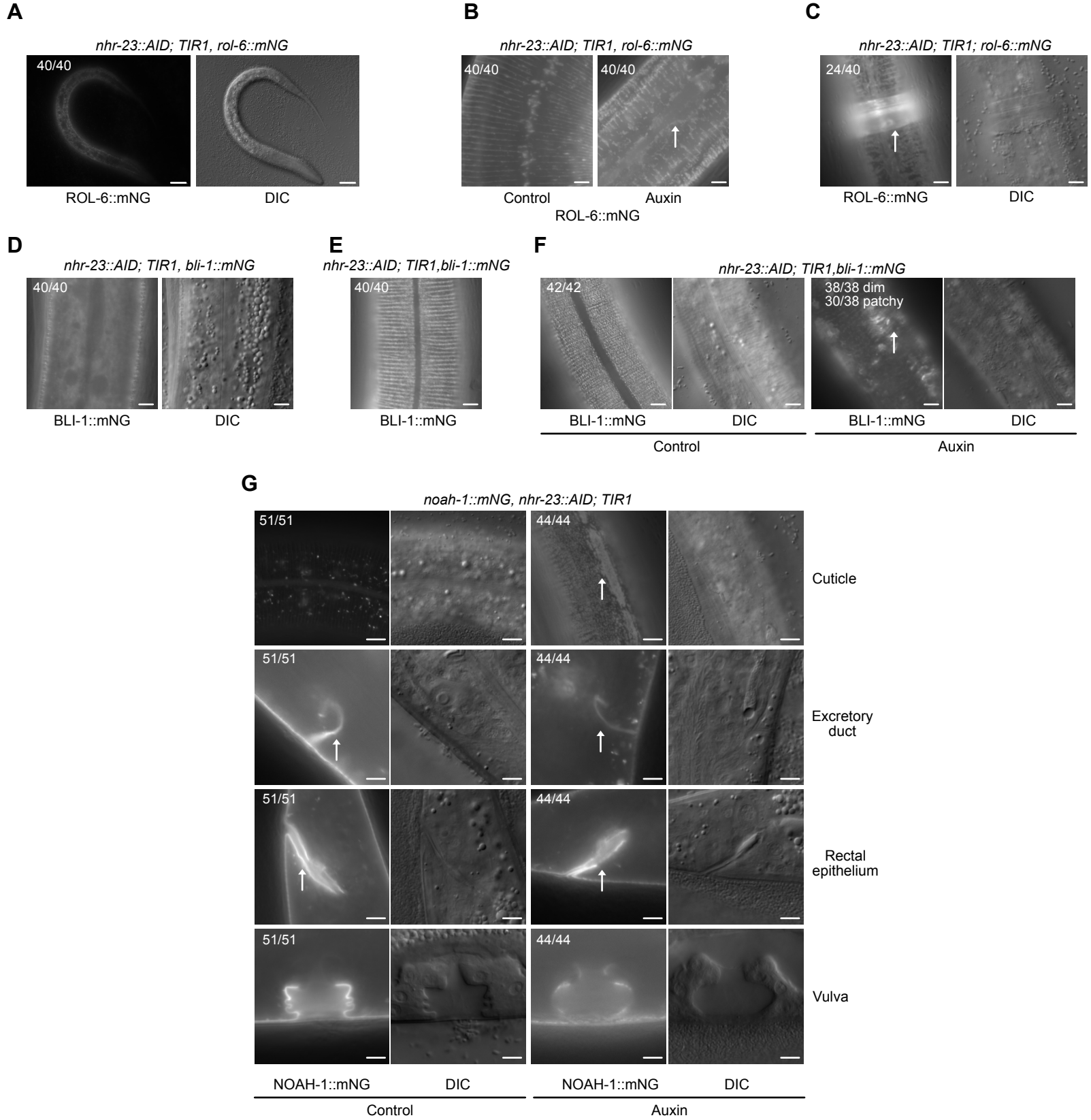
A
nhr-23::AID; TIR1, rol-6::mNG
40/40
ROL-6::mNG
DIC
B
nhr-23::AID; TIR1, rol-6::mNG
40/40
40/40
Control
Auxin
ROL-6::mNG
C
nhr-23::AID; TIR1; rol-6::mNG
24/40
ROL-6::mNG
DIC
D
nhr-23::AID; TIR1, bli-1::mNG
40/40
BLI-1::mNG
DIC
E
nhr-23::AID; TIR1,bli-1::mNG
40/40
BLI-1::mNG
F
nhr-23::AID; TIR1,bli-1::mNG
42/42
38/38 dim
30/38 patchy
BLI-1::mNG
DIC
BLI-1::mNG
DIC
Control
Auxin
G
noah-1::mNG, nhr-23::AID; TIR1
51/51
44/44
Cuticle
Excretory duct
Rectal epithelium
Vulva
NOAH-1::mNG
DIC
NOAH-1::mNG
DIC
Control
Auxin

**Figure 6**

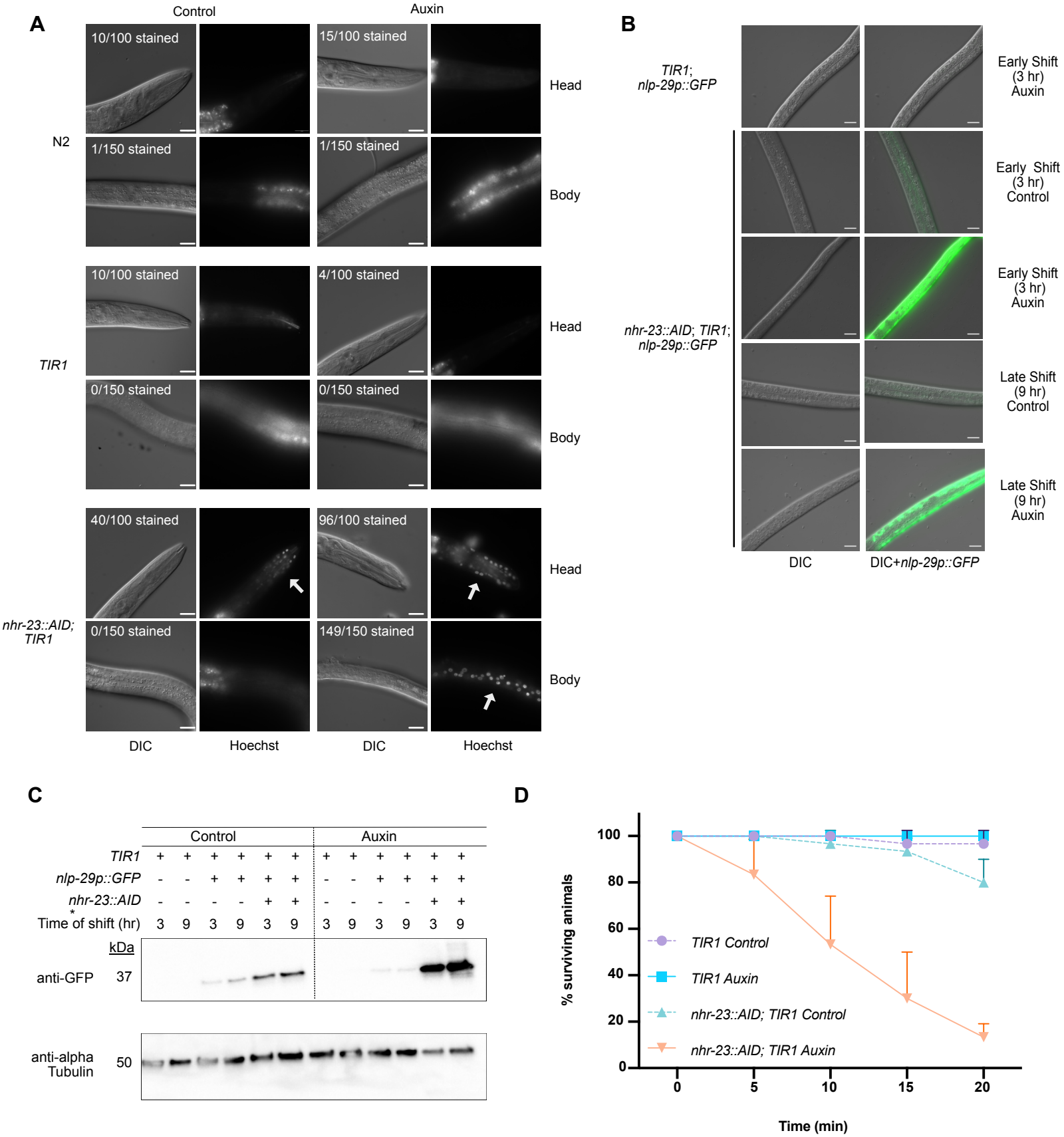
A
Control
Auxin
10/100 stained
15/100 stained
Head
N2
1/150 stained
1/150 stained
Body
10/100 stained
4/100 stained
Head
TIR1
0/150 stained
0/150 stained
Body
40/100 stained
96/100 stained
Head
nhr-23::AID; TIR1
0/150 stained
149/150 stained
Body
DIC
Hoechst
DIC
Hoechst
B
TIR1; nlp-29p::GFP
Early Shift (3 hr) Auxin
Early Shift (3 hr) Control
nhr-23::AID; TIR1; nlp-29p::GFP
Early Shift (3 hr) Auxin
Late Shift (9 hr) Control
Late Shift (9 hr) Auxin
DIC
DIC+nlp-29p::GFP
C
Control
Auxin
TIR1 + + + + + + + + + + + +
nlp-29p::GFP - - + + + + - - + + + +
nhr-23::AID - - - - + + - - - - + +
Time of shift (hr) 3 9 3 9 3 9 3 9 3 9 3 9
kDa
anti-GFP 37
anti-alpha Tubulin 50
D
% surviving animals
100
80
60
40
20
0
TIR1 Control
TIR1 Auxin
nhr-23::AID; TIR1 Control
nhr-23::AID; TIR1 Auxin
0
5
10
15
20
Time (min)

**Figure 7**

**A**

| Strain | Promoter for tissue-specific RNAi | Tissue-specific RNAi | RNAi | N |
|---|---|---|---|---|
| N2 | N/A | Whole animal | Control | 362 |
| | | | *nhr-23* | 272 |
| WM118 | *myo-2p* | Body muscle | Control | 252 |
| | | | *nhr-23* | 320 |
| VP303 | *nhx-2p* | Intestine | Control | 317 |
| | | | *nhr-23* | 393 |
| MGH171 | *vha-6p* | Intestine | Control | 602 |
| | | | *nhr-23* | 573 |
| JU2039 | *lin-31p* | Vulval precursor cells | Control | 325 |
| | | | *nhr-23* | 367 |
| QK52 | *wrt-2p* | Seam cell, hypodermis, rectum | Control | 299 |
| | | | *nhr-23* | 198 |
| JDW371 | *SCMp* | Seam cell, some hypodermal | Control | 232 |
| | | | *nhr-23* | 153 |
| JDW510 | *suro-1p* | Hypodermis | Control | 259 |
| | | | *nhr-23* | 211 |

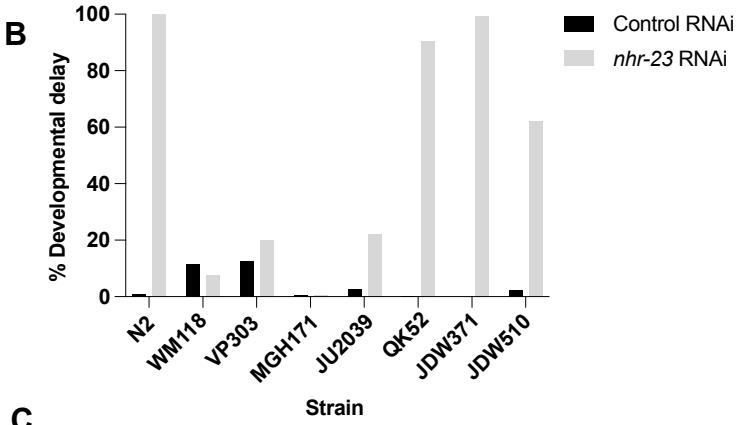


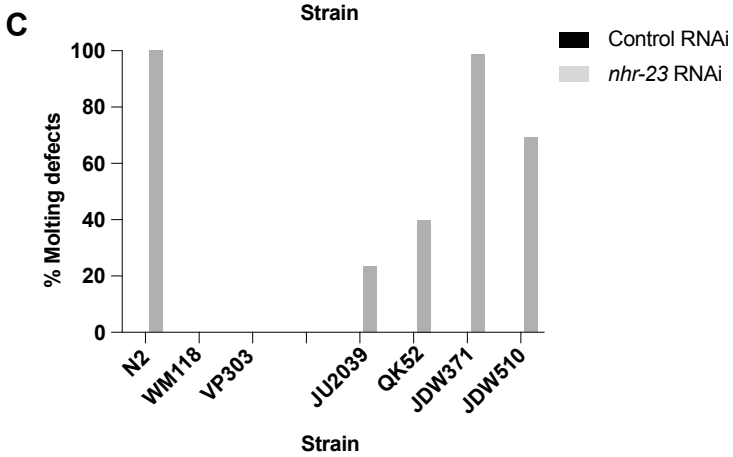


**D**

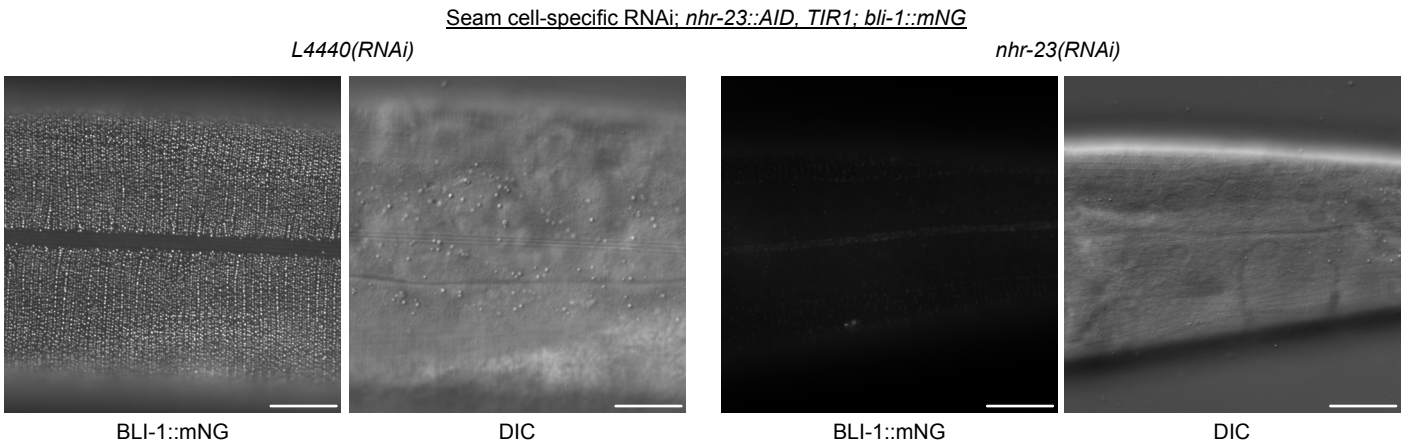


**Figure 8**

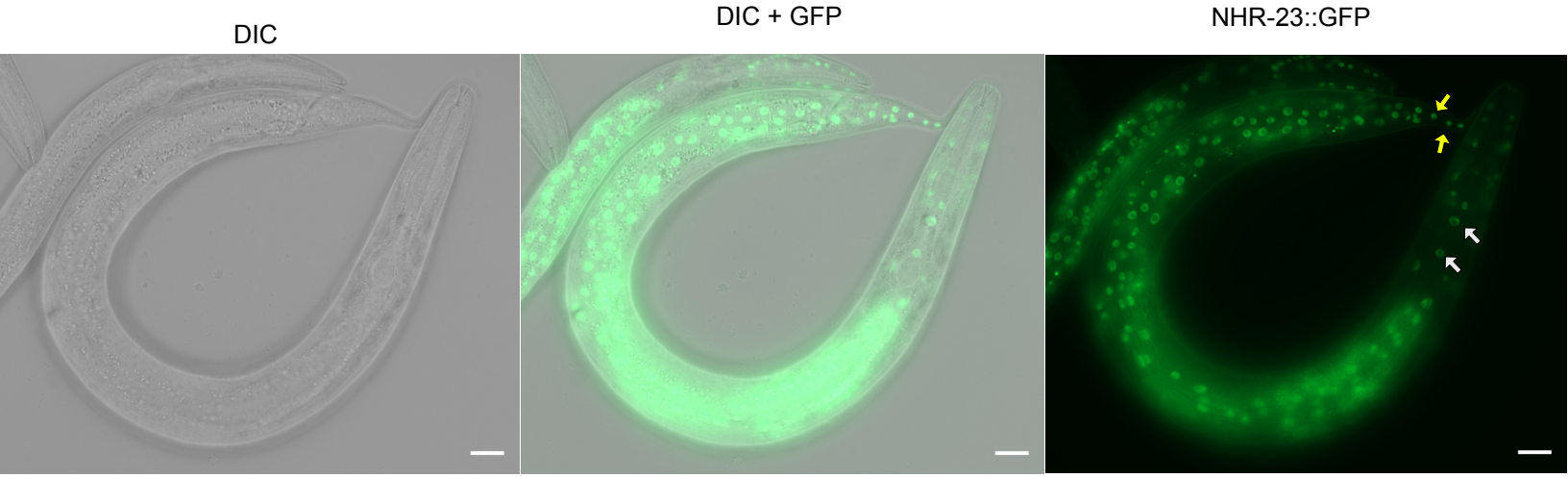


**Figure S1**

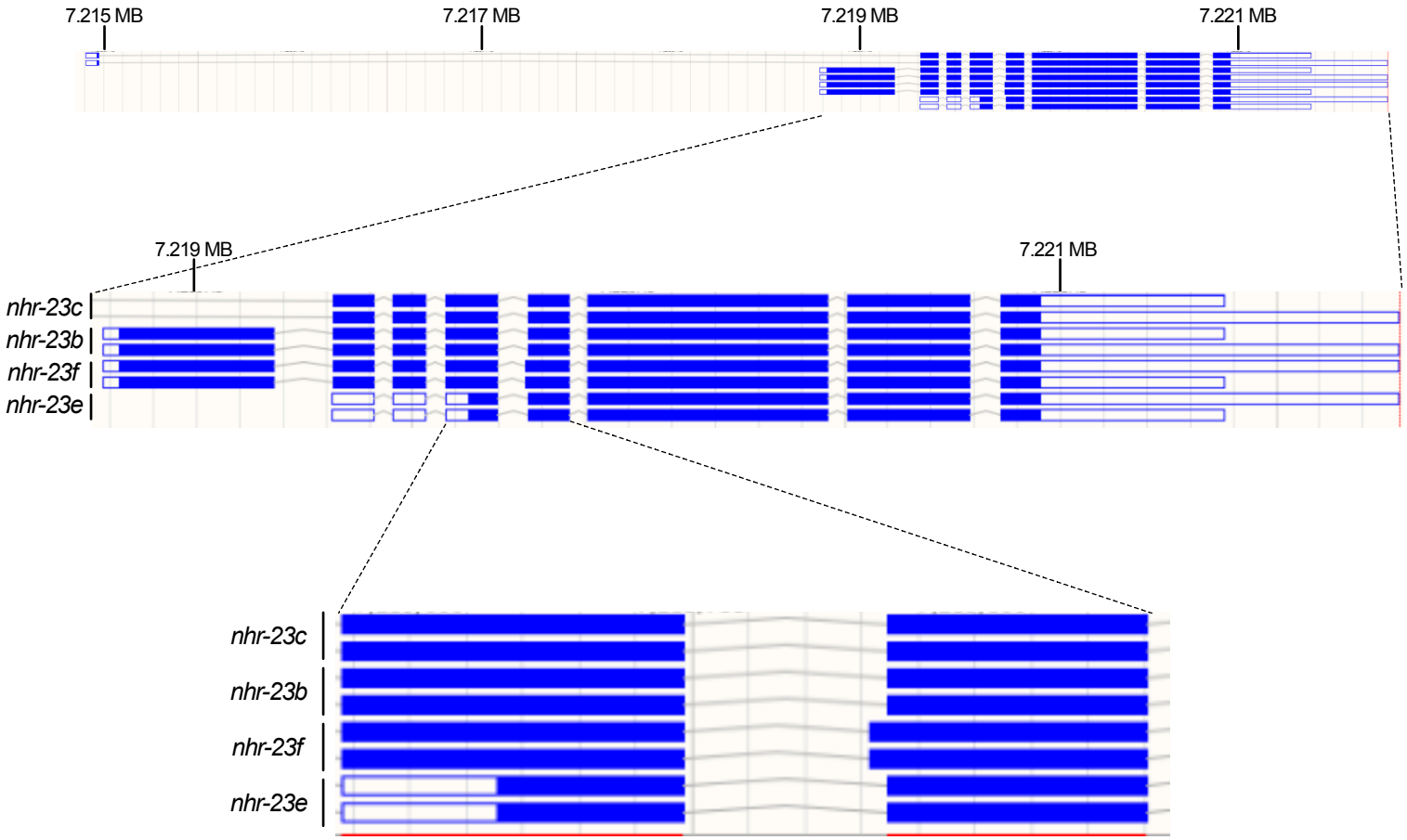
7.215 MB
7.217 MB
7.219 MB
7.221 MB
7.219 MB
7.221 MB
nhr-23c
nhr-23b
nhr-23f
nhr-23e
nhr-23c
nhr-23b
nhr-23f
nhr-23e

**Figure S2**

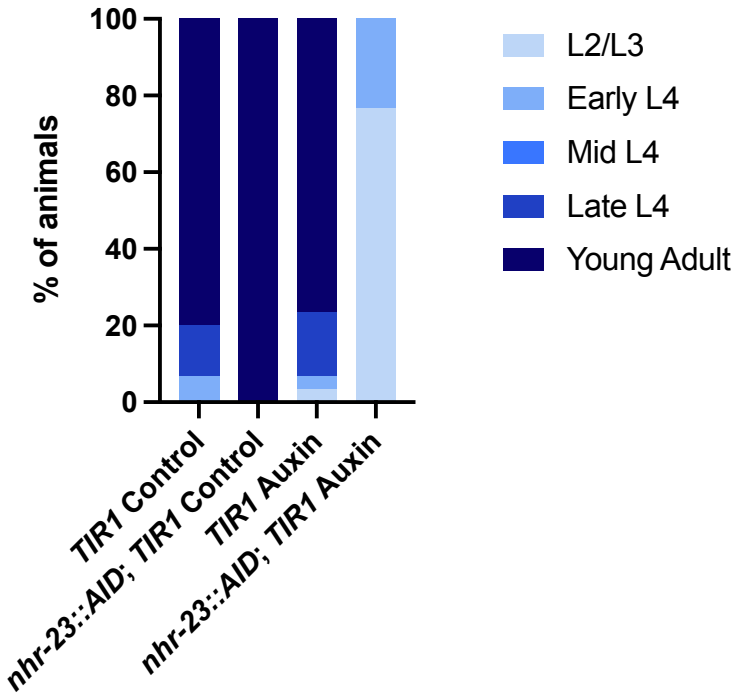
100
80
60
40
20
0
% of animals
TIR1 Control
nhr-23::AID; TIR1 Control
TIR1 Auxin
nhr-23::AID; TIR1 Auxin
L2/L3
Early L4
Mid L4
Late L4
Young Adult

**Figure S3**

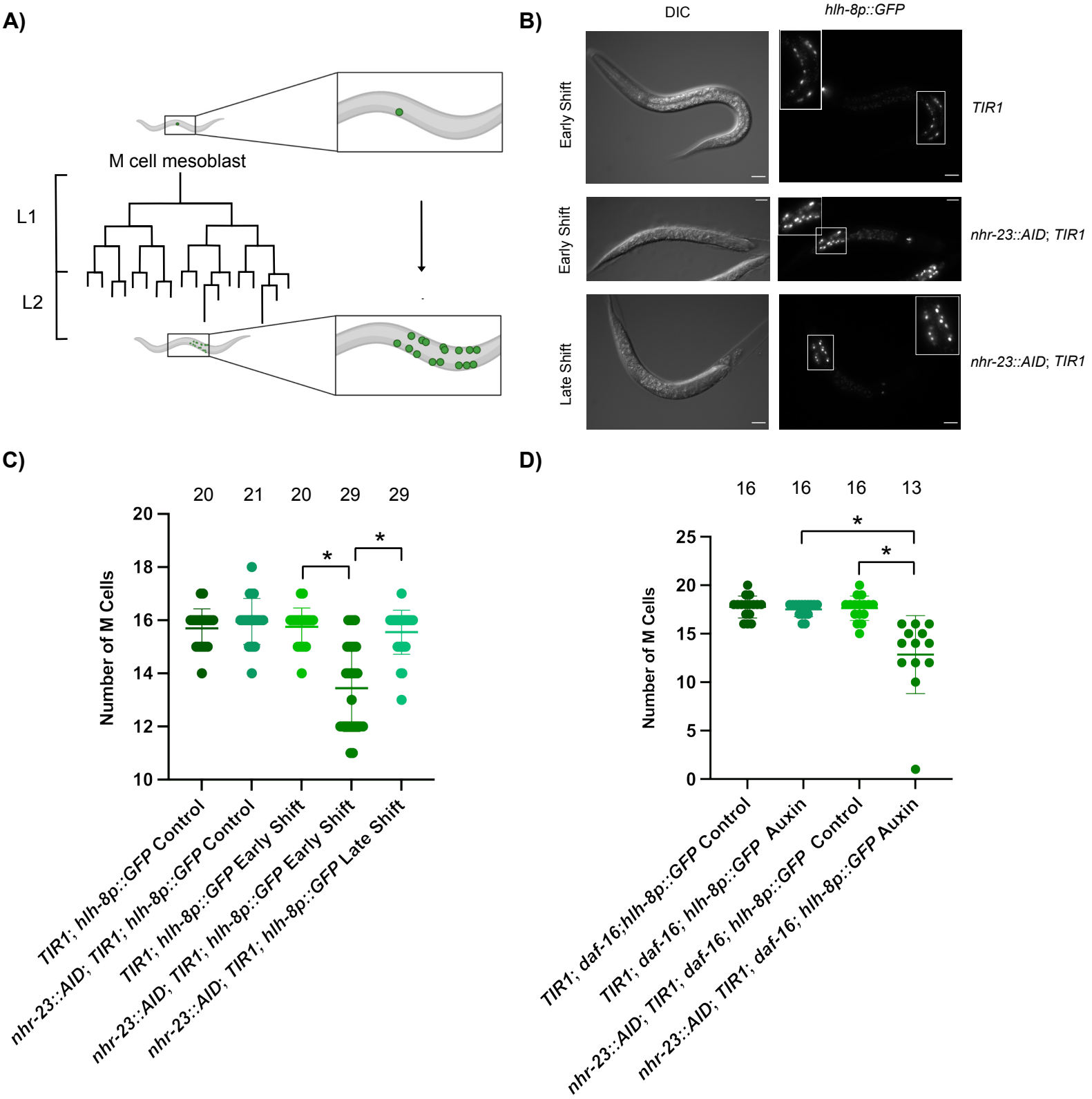
A)
M cell mesoblast
L1
L2
B)
DIC
hlh-8p::GFP
Early Shift
Early Shift
Late Shift
TIR1
nhr-23::AID; TIR1
nhr-23::AID; TIR1
C)
20 21 20 29 29
Number of M Cells
TIR1; hlh-8p::GFP Control
nhr-23::AID; TIR1; hlh-8p::GFP Control
TIR1; hlh-8p::GFP Early Shift
nhr-23::AID; TIR1; hlh-8p::GFP Early Shift
nhr-23::AID; TIR1; hlh-8p::GFP Late Shift
D)
16 16 16 13
Number of M Cells
TIR1; daf-16;hlh-8p::GFP Control
TIR1; daf-16; hlh-8p::GFP Auxin
nhr-23::AID; TIR1; daf-16; hlh-8p::GFP Control
nhr-23::AID; TIR1; daf-16; hlh-8p::GFP Auxin

**Figure S4**

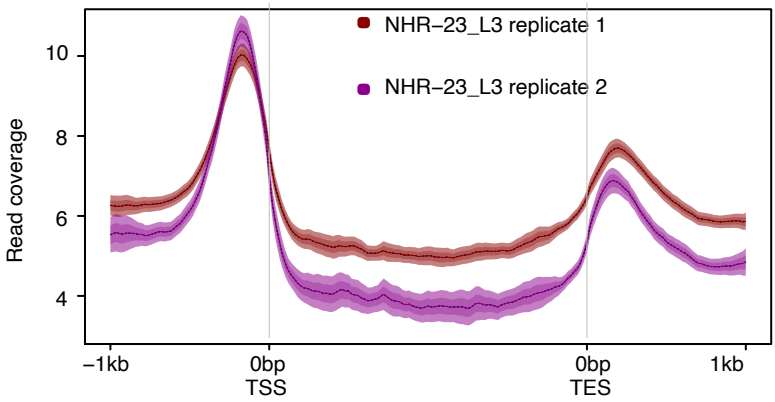
NHR−23_L3 replicate 1
NHR−23_L3 replicate 2
Read coverage
10
8
6
4
−1kb
0bp
TSS
0bp
TES
1kb

**Figure S5**

**A**

| Genotype | Brood size (±std. dev.) |
|---|---|
| Wild type | 290±48 |
| *nhr-23::AID; TIR1, rol-6::mNG* | 293±48 |
| *nhr-23::AID; TIR1, bli-1::mNG* | 236±56 |
| *noah-1::mNG, nhr-23::AID; TIR1* | 246±27 |

**B**

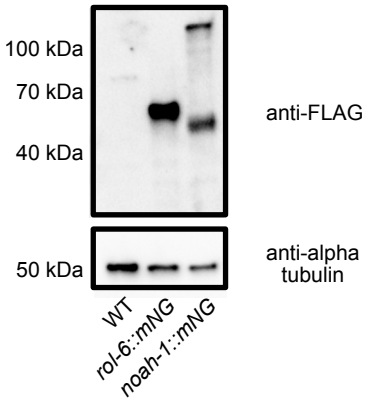


**C**

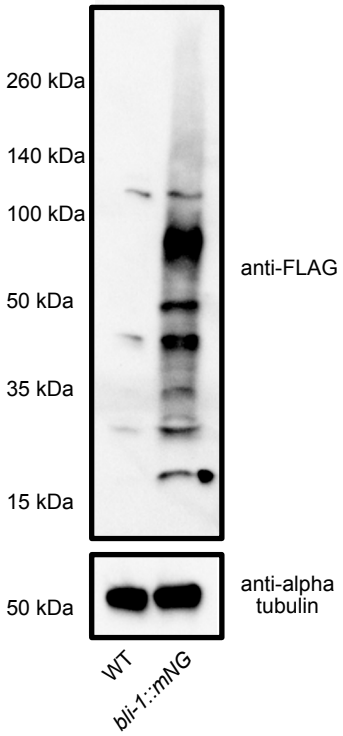


**Figure S6**

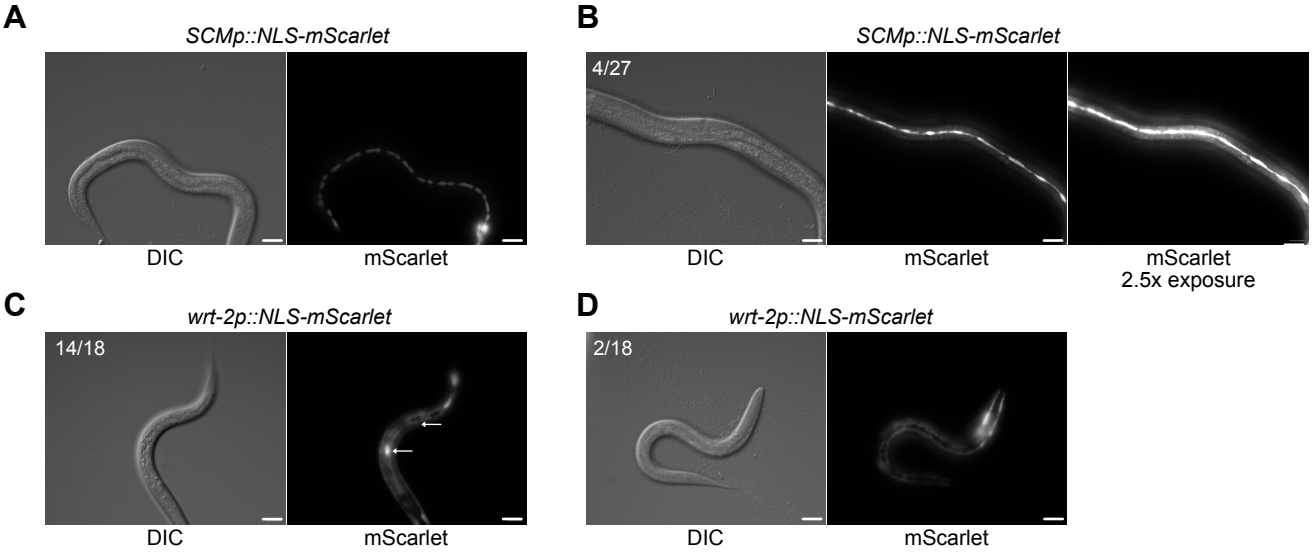
A
SCMp::NLS-mScarlet
DIC
mScarlet
B
SCMp::NLS-mScarlet
4/27
DIC
mScarlet
mScarlet
2.5x exposure
C
wrt-2p::NLS-mScarlet
14/18
DIC
mScarlet
D
wrt-2p::NLS-mScarlet
2/18
DIC
mScarlet

**Figure S7**

## Control

HIS-72::mNeonGreen

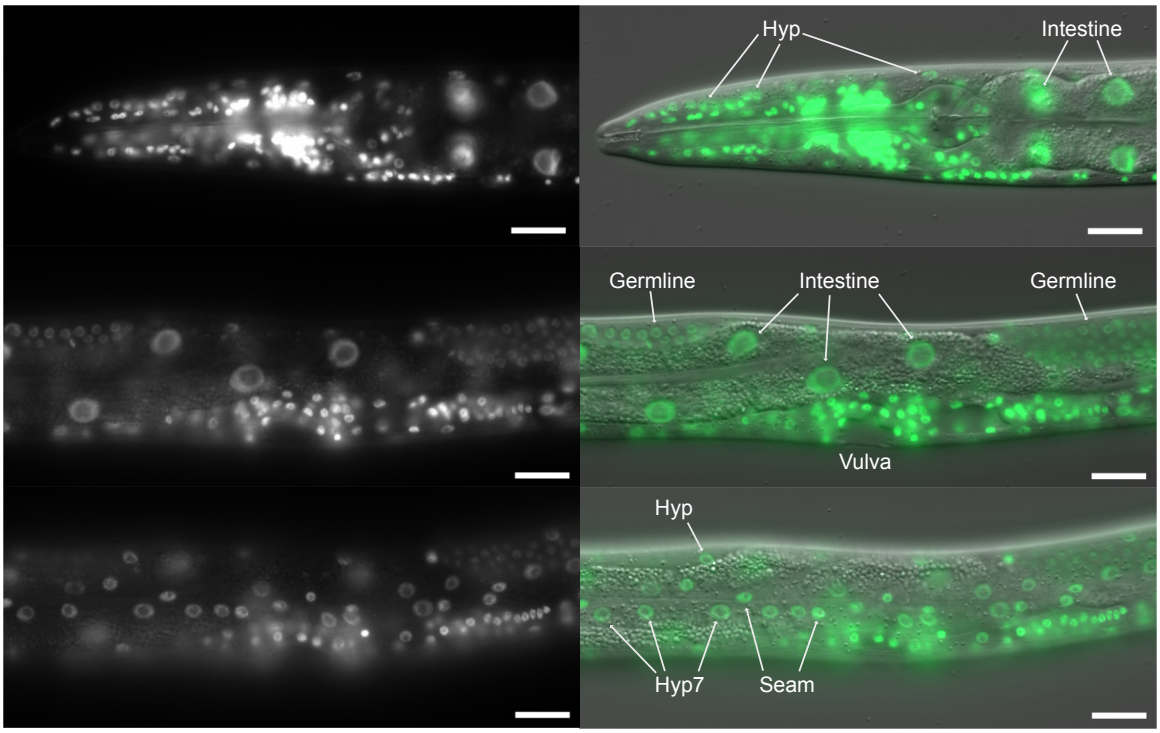


## mNeonGreen RNAi

HIS-72::mNeonGreen

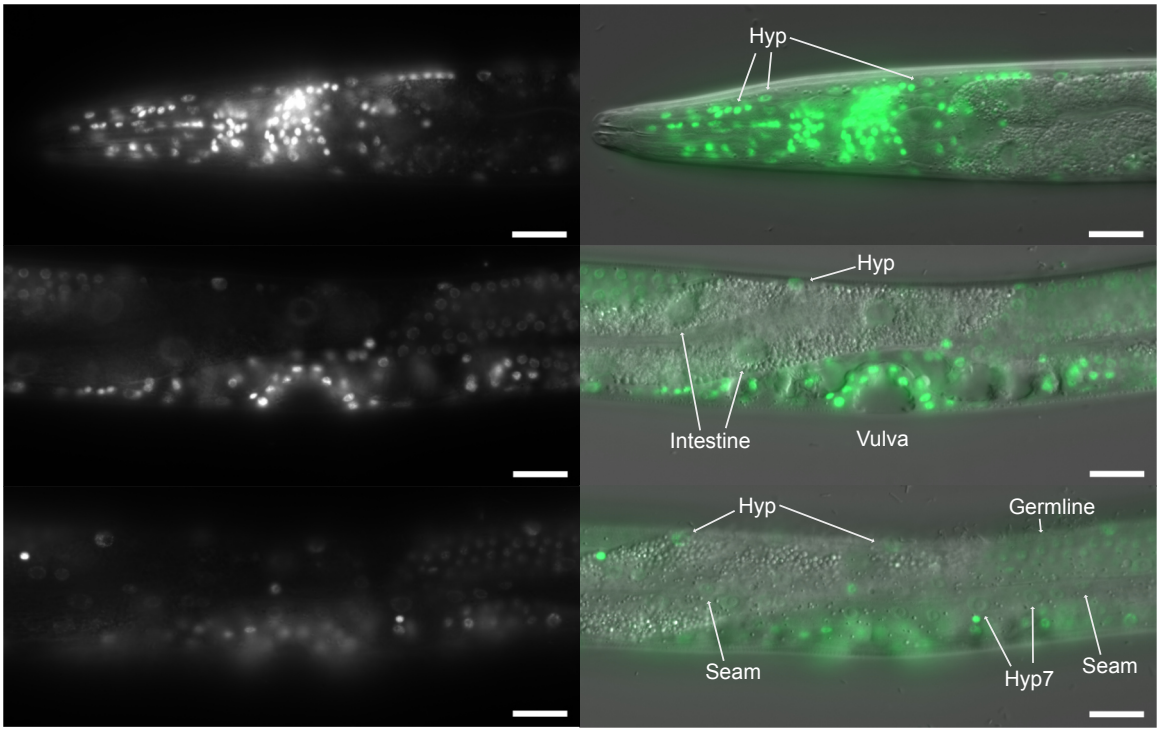


**Figure S8**